Journal of Advanced Research 59 (2024) 19–33

Contents lists available at ScienceDirect

Journal of Advanced Research

journal homepage: www.elsevier.com/locate/jare

Salicylic acid-doped iron nano-biostimulants potentiate defense responses and suppress Fusarium wilt in watermelon

Muhammad Noman [a], Temoor Ahmed [a,b], Muhammad Shahid [c], Muhammad Mudassir Nazir [d], Azizullah [a], Dayong Li [a], Fengming Song [a,*]

[a] State Key Laboratory of Rice Biology and Ministry of Agriculture Key Laboratory of Molecular Biology of Crop Pathogens and Insects, Institute of Biotechnology, College of Agriculture and Biotechnology, Zhejiang University, Hangzhou 310058, China
[b] Xianghu Laboratory, Hangzhou 311231, China
[c] Department of Bioinformatics and Biotechnology, Government College University, Faisalabad 38000, Pakistan
[d] School of Environment and Safety Engineering, Jiangsu University, Zhenjiang 212013, China

HIGHLIGHTS

- Bio-FeNPs and SINCs supplement watermelon growth.
- Soil drenching with bio-FeNPs and SINCs restrict invasive fungal growth.
- Bio-FeNPs and SINCs modulate oxidative signaling in watermelon.
- Bio-FeNPs and SINCs trigger defense responses in watermelon against Fusarium wilt.

GRAPHICAL ABSTRACT

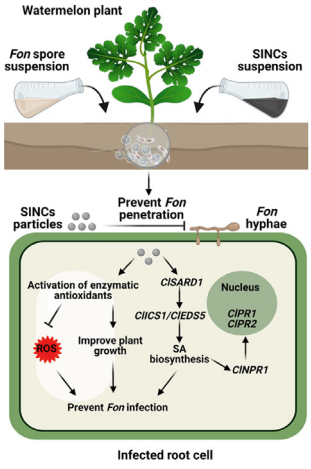

ARTICLE INFO

Article history:
Received 28 March 2023
Revised 7 June 2023
Accepted 25 June 2023
Available online 28 June 2023

Keywords:
Fusarium wilt
Innate immunity
Iron nanocomposites
Salicylic acid
Watermelon

ABSTRACT

Introduction: Chemo- and bio-genic metallic nanoparticles (NPs), as a novel nano-enabled strategy, have demonstrated a great potential in crop health management.
Objective: The current study aimed to explore the efficacy of advanced nanocomposites (NCs), integrating biogenic (bio) metallic NPs and plant immunity-regulating hormones, in crop disease control.
Methods: Iron (Fe) NPs were biosynthesized using cell-free supernatant of a Fe-resistant strains, *Bacillus marisflavi* ZJ-4. Further, salicylic acid-coated bio-FeNPs (SI) NCs were prepared *via* co-precipitation method under alkaline conditions. Both bio-FeNPs and SINCs were characterized using basic analytical techniques, including Fourier transform infrared (FTIR) spectroscopy, X-ray diffraction analysis, and scanning/transmission electron microscopy.
Results: Bio-FeNPs and SINCs had variable shapes with average sizes of 72.35 nm and 65.87 nm, respectively. Under greenhouse conditions, bio-FeNPs and SINCs improved the agronomic traits of the watermelon plants, and SINCs outperformed bio-FeNPs, providing the maximum growth promotion of 32.5%. Soil-drenching with bio-FeNPs and SINCs suppressed *Fusarium oxysporum* f. sp. *niveum*-caused Fusarium wilt in watermelon, and SINCs provided better protection than bio-FeNPs, through inhibiting

* Corresponding author.
E-mail address: fmsong@zju.edu.cn (F. Song).

https://doi.org/10.1016/j.jare.2023.06.011

the fungal invasive growth within host plants. SINCs improved the antioxidative capacity and primed a systemic acquired resistance (SAR) response *via* activating the salicylic acid signaling pathway genes. These findings indicate that SINCs can reduce the severity of Fusarium wilt in watermelon by modulating antioxidative capacity and potentiating SAR to restrict *in planta* fungal invasive growth.

Conclusion: This study provides new insights into the potential of bio-FeNPs and SINCs as biostimulants and bioprotectants for growth promotion and Fusarium wilt suppression, ensuring sustainable watermelon production.

Introduction

Fusarium wilt, caused by *Fusarium oxysporum* f. sp. *niveum* (*Fon*), is a devastating threat to the watermelon (*Citrullus lanatus* L.) productivity worldwide, leading to significant reductions in yield and quality [1]. This soil-borne pathogenic fungus infects through the roots and attacks the vascular system of its host plants, leading to wilting, yellowing, and ultimately death of the infected plants [2]. The infected plants generally do not exhibit any visible disease symptom during the early stage of infection, and once disease symptoms appear, it is hard to cure the diseased plants by applying traditional chemical pesticides. Furthermore, *Fon* can persistently survive in the soil for many years and accumulate to a high level of inoculum, particularly in the greenhouse monocropping system, making its infection difficult to prevent [2]. An integrated control strategy coupling the use of disease-resistant varieties, crop rotation, and chemical pesticides has been shown to moderately alleviate the incidence and severity of Fusarium wilt in watermelon [3]. However, highly effective targeted control strategies remain an ongoing challenge.

Nano-enabled strategies for crop disease management are an emerging field of research that harnesses the unique properties, such as size, shape, and surface area-to-volume ratio, of nanoparticles (NPs) to combat plant diseases. Nanoscale materials, such as nanopesticides, have shown great potential for the development of effective and sustainable disease management practices [4,5]. For example, *Trichoderma longibrachiatum*-synthesized silver NPs at 0.25 mM concentration suppressed Fusarium wilt in tomato, caused by *F. oxysporum* f. sp. *lycopersici*, *via* direct pathogen inhibition [6]. In another study, chemical-based copper NPs reduced the disease severity index of Fusarium wilt of chrysanthemum up to 32 %, caused by *F. oxysporum* f. sp. *chrysanthemi* [7]. Seed treatment and foliar application of the lanthanum oxide NPs significantly suppressed cucumber Fusarium wilt, caused by *F. oxysporum* f. sp. *cucumerinum* [8]. Iron (Fe) is an essential micronutrient for both plants and pathogens, playing vital roles in various physiological processes, including respiration and DNA synthesis. Plants have evolved sophisticated strategies to regulate Fe uptake, distribution, and utilization to maintain their metabolic processes and restrict its availability to pathogens [9]. Despite its key roles in plant metabolism, the specific role of FeNPs in combating plant diseases remains elusive. Recently, biogenic (bio)-FeNPs have been shown to possess antimicrobial properties against various phytopathogens and their potential application in plant disease control has recently been explored [5]. For example, microalga-stabilized FeNPs exhibited significant antifungal activity against *F. oxysporum* and *Rhizoctonia solani* [10]. Similarly, phytogenic FeNPs suppressed Fusarium wilt in tomato *via* inhibiting pathogen growth and triggering host defense response [11]. In addition to plant defense activation against pathogen [5], bio-FeNPs can also directly interact with pathogens, disrupting their cellular integrity or essential metabolic processes, thereby inhibiting their growth and development. For example, bio-FeNPs showed tremendous antifungal activity against *Sclerotinia sclerotiorum*, inhibiting its growth and sclerotia germination [12]. The successful implementation of bio-FeNPs in plant disease management highlights that these nano-enabled approaches can revolutionize the crop protection system by providing highly effective, eco-friendly, and sustainable disease management strategies [4]. Bacteria-mediated synthesis of FeNPs is the mostly exploited green route due to its versatility, simplicity, and high yields. Several Fe-resistant bacterial strains, including *Actinobacter* spp., *Geobacter metallireducens*, and *Bacillus aryabhattai*, have been reported for the synthesis of FeNPs [5,13].

The use of nanoscale delivery systems for agrochemicals, such as nutrients and pesticides, has shown tremendous potential in improving plant growth and defense against fungal pathogens [14,15]; however, potential benefits of therapeutic delivery of phytohormones using nano-carriers remain to be established. Salicylic acid (SA) is one of the key phytohormones that mediates a complicated signaling network to activate defense responses against biotic stress, including fungal diseases [16,17]. Exogenous application of SA and its structural analogs has become an attractive way to induce systemic acquired resistance (SAR), a well-established form of inducible immunity in plants. SAR provides plants with systemic, broad-spectrum, and long-lasting protection against diverse pathogens [18,19]. For example, the exogenous application of SA or acibenzolar-S-methyl to cucumber and soybean plants activated their defense against scab, caused by *Cladosporium cucumerinum*, and damping-off, caused by *Fusarium solani*, respectively, through enhancing the expression of defense-related genes and reducing oxidative stress [20,21]. Recently, it has been reported that SA can suppress Fusarium wilt and root-knot in watermelon *via* activating defense pathways and engineering the rhizosphere microbiome [22–25]. Given these facts, SA-loaded NPs can be used as a novel approach to sustainably improve plant defense responses *via* leveraging the unique properties of NPs and the regulation of phytohormone signaling. However, mechanistic insights regarding the cumulative function of SA and bio-NPs in plant disease management are still lacking.

The primary aim of this study was to reconnoiter the possibility and efficacy of nanocomposites (NCs), integrating bio-NPs with plant immunity-regulating hormones, in crop disease management. To this end, we first prepared bio-FeNPs using *Bacillus marisflavi* ZJ-4, and then encapsulated these bio-FeNPs with SA to generate SA-loaded bio-Fe (SI) NCs. Disease assays were conducted, along with a series of physiological, morphological, and gene expression analyses, to investigate the efficacy of SINCs in preventing Fusarium wilt in watermelon. This study provides valuable insights into an innovative nano-enabled approach for achieving sustainable control of crop diseases.

Materials and methods

Fe-resistant bacterial strain isolation and molecular characterization

Rhizosphere soil samples from watermelon plants grown in a field in Hangzhou, China (29° 56′ 42″ N and 119° 35′ 54″ E) were collected and subjected to serial dilution for isolating the Fe-resistant bacterial strain *B. marisflavi* ZJ-4, following a previous protocol

[26]. Briefly, 1 g of rhizosphere soil was serially diluted, and 100 µL of two different dilutions (10^{-3} and 10^{-5}) was spread on nutrient agar plates, which were then incubated at 28 ± 2 °C for 2 d. The bacterial strains with unique morphological characteristics, such as shape, color, size, and texture, were acquired and purified through repeated streaking. The minimum inhibitory concentration (MIC) method was applied to identify the highly-resilient bacterial isolates towards anhydrous ferrous sulfate ($FeSO_4{\cdot}7H_2O$, 99% purity; Sinopharm Chemical Reagent Ltd., Shanghai, China), following the previous method [27]. The extraction of genetic material was performed using a DNA extraction kit (Sangon Biotech, Shanghai, China) according to the instruction manual. For taxonomic characterization of the bacterial strain, the *RNA polymerase subunit B* (*rpoB*) gene was selected along with *16S rRNA*, a commonly used taxonomic marker, because it is highly conserved among bacteria and contains variable regions that can be used for species-level identification [28]. The amplification of *16S rRNA* and *rpoB* genes was conducted utilizing the previously published fD1 and rD1 [29] and rpoB-F and rpoB-R [28] primer pairs, respectively (Table S1). The amplified sequences were purified and sequenced commercially (Zhejiang Youkang Biotech, Hangzhou, China). Final sequences were analyzed and compared to other homologues in the database using the online BLASTn tool. Alignment of the sequences was executed using ClustalW and the phylogenetic tree was generated through the Maximum Likelihood method utilizing MEGA7 software (v7.0) with 1000-bootstrap replicates.

Synthesis of bio-FeNPs and SINCs

The extracellular production of bio-FeNPs was performed using the culture supernatant of *B. marisflavi* strain ZJ-4 as described previously [30], with slight modifications. Briefly, the Fe-resistant *B. marisflavi* strain ZJ-4 was grown in nutrient broth at 28 ± 2 °C with shaking at 150 rpm for 24 h. To produce FeNPs, a mixture was prepared by combining 100 mL of 10 mM $FeSO_4{\cdot}7H_2O$ and a similar volume of *B. marisflavi* strain ZJ-4 cell-free supernatant obtained through centrifugation at 6,000 *g* for 10 min. The reaction mixture was then incubated at 28 ± 2 °C with shaking at 200 rpm for 72 h and centrifuged at 10,000 *g* for 15 min, yielding a bio-FeNPs pellet. The pellet was then freeze-dried for 6 h to remove moisture and finely ground into a powder using a sterilized pestle and mortar, facilitating easier handling and sample preparation for further analyses. The fine powder was then stored in an airtight container for subsequent analyses. Media lacking the bacterial culture filtrate and cell-free filtrate lacking $FeSO_4{\cdot}7H_2O$ were utilized as blanking controls to account for the baseline absorbance of the media components or ionic substrate used in the experiments. The obtained bio-FeNPs were purified by repeated washing with ddH_2O, following the previously described method [30].

The synthesis of SINCs was carried out by following an earlier method [31]. Briefly, bio-FeNPs were mixed in 250 mL aqueous solution of SA (99% purity, Sigma-Aldrich, St. Louis, MO, USA) with a ratio of 2FeNPs:4SA (w/w) under vigorous shaking at 200 rpm using an orbital shaker, ensuring thorough mixing and homogeneity of the components. The mixture was then precipitated under alkaline conditions (∼pH 11 and 50 °C) using potassium hydroxide. The precipitates were subjected to multiple washing steps and magnetic separation to remove any potential impurities originating from the uncoated bio-FeNPs, KOH and SA. These additional steps were implemented to ensure the purity of the final SINCs product.

Characterization of bio-FeNPs and SINCs

The presence of the bio-FeNPs in the reaction mixture was confirmed by scanning within 200–800 nm wavelength region using an ultraviolet–visible (UV–vis) spectrophotometer (Model 2550, Shimadzu, Nakagyo-ku, Kyoto, Japan) [32]. The interfacial features and functional groups responsible for the stability of bio-FeNPs and SINCs were analyzed in the spectral region from 4000 to 500 cm^{-1} using Fourier transform infrared (FTIR) spectroscopy (Thermo Scientific NICOLET iS50FT-IR, Waltham, MA, USA) [33]. The X-ray diffraction (XRD) analysis (XPertPro diffractometer, Almelo, the Netherlands) was performed to determine the crystallinity of FeNPs and SINCs, which was conducted at 10-80° 2θ diffraction angle, operating at 45 KeV of working voltage and 40 mA of current [34]. The scanning/transmission electron microscopy (SEM: TM1000, Hitachi, Tokyo, Japan; TEM: JEOL JEM-1230, Tokyo, Japan) techniques were utilized to determine the surface morphology and size of the FeNPs and SINCs [35]. To prepare samples for SEM and TEM, an aluminum stub and a carbon-coated copper grid were utilized, respectively. The metallic content/fractions of the bio-FeNPs and SINCs were evaluated by energy dispersive X-ray spectrum (EDS; Oxford Instruments EDS Model, High Wycombe, Buckinghamshire, UK) analysis, with 20 KeV of working voltage.

Absorptiometric determination of Fe and SA in NPs

Spectroscopic analysis was performed to quantify Fe and SA in bio-FeNPs and SINCs in ddH_2O as described previously [5,36]. Briefly, bio-FeNPs and SINCs at 100 µg/mL were dispersed in ddH_2O under vigorous shaking for 30 min. The suspensions were purified through Whatman no. 1 filter paper to eliminate suspended particulate impurities, and absorption spectra were obtained at 296 nm and 305 nm to estimate SA and Fe amount, respectively, using an UV–vis spectrophotometer. Controls were prepared containing pure SA and $FeSO_4{\cdot}7H_2O$.

In vitro dissolution of bio-FeNPs and SINCs

In vitro metal release rate of bio-FeNPs and SINCs at a concentration of 25 µg/mL was determined using sterile ddH_2O (pH 7.0) and potting mix extract (pH 5.0), following a previously described protocol [37]. Briefly, potting mix extract was obtained by shaking 50 g potting mix in 200 mL ddH_2O at 26 °C 150 rpm for 2 h, which was then purified by removing suspended potting mix particles through filtration using double-layered cheesecloth. Bio-FeNPs and SINCs were suspended in sterile ddH_2O and potting mix extract and kept at 26 ± 2 °C with shaking at 150 rpm. An aliquot of 1 mL was taken out from each suspension at designated time points (1, 6, 12, and 24 h). The samples were centrifuged, and the resultant filtrates were filtered using a 0.22 µm injection filter to remove suspended particulates. The purified filtrates were acid digested using $HClO_4$: HNO_3 (1:3) and underwent inductively coupled plasma-mass spectrometry (ICP-MS; Optima8000DV, Perkin Elmer, Waltham, MA, USA) for Fe quantification, providing metal release behavior of bio-FeNPs and SINCs in different media with variable compositions (*i.e.,* ddH_2O and potting mix).

Experimental setup and plant materials

In all experiments, two-week-old watermelon (var. Zaojia) plants, which were grown in a potting mix, containing vermiculite: plant ash: perlite (in a volume ratio of 6:2:1, respectively), were utilized. The watermelon plants were subjected to 5 different treatments, including ddH_2O, $FeSO_4{\cdot}7H_2O$ (as a Fe ions source), SA, bio-FeNPs, and SINCs. Specifically, experimental plants were treated with bio-FeNPs and SINCs suspensions in ddH_2O (50 mL per pot with 3 plants) *via* soil drenching, reaching a final concentration of ∼ 100 mg/Kg of potting mix per pot, as reported previously [38,39]. Control plants were supplied with sterile ddH_2O and similar concentrations (*i.e.,* 100 mg/Kg) of $FeSO_4{\cdot}7H_2O$ or SA.

The experiments were set in a completely randomized design. Each treatment had three replicates, and the experimental plants were grown for 15 d under an 8-h dark/16-h light cycle at a temperature of 22 °C and a relative humidity of 65%.

Watermelon growth, Fe content, and physiological parameters

Watermelon plants were harvested at 15 d post-treatment with NPs and washed to remove adhered potting mix particles, followed by the estimation of growth characteristics, including plant height and fresh and dry weights. The plant samples were oven-dried overnight at 80 ℃, and their dry weight was measured. The oven-dried roots and shoots were subjected to acid digestion using $HClO_4$:HNO_3 (1:3) for 48 h and diluted with ddH_2O to a final volume of 15 mL. The Fe content in the root and shoot tissues was quantified using ICP-MS [40]. The translocation factor (TF), which represents the ratio of shoot Fe concentration to root Fe concentration, was computed to assess the distribution of Fe from roots to shoots. TF provides valuable information regarding the efficiency of Fe translocation within the plant system.

For physiological assays, plant samples were collected at 15 d post-treatment, frozen in liquid nitrogen, and stored at −80 °C until downstream processing. The reactive oxygen species (ROS) generation was measured calorimetrically using the titanium sulfate reagent method for hydrogen peroxide (H_2O_2), hydroxylamine oxidation method for superoxide anion free radical ($O_2^{\bullet-}$), and thiobarbituric acid method for malondialdehyde (MDA) according to previously described protocols [41–43]. Briefly, the root and shoot tissues (200 mg) were pulverized in 1 mL of potassium phosphate buffer (65 mM and pH 7.8) and then centrifuged at 4 °C for 10 min at 5,000 *g*. The absorbance was measured at 430 nm for H_2O_2, 530 nm for $O_2^{\bullet-}$, and 532 nm for MDA using an UV–vis spectrophotometer. The activity of enzymes in root and shoot tissues (500 mg) was estimated by pulverizing the tissue in 1 mL of ice-cooled phosphate buffer (50 mM and pH 7.0), centrifuged for 10 min at 12,000 *g* at 4 °C, and subjected to UV–vis spectrophotometry to estimate the activities of catalase (CAT), peroxidase (POD), and superoxide dismutase (SOD) at 520 nm, 470 nm, and 560 nm, respectively, following previously described protocols [44,45].

Fon inoculum preparation, disease assays, and in planta growth estimation

Fon inoculum was prepared by culturing 7-d-old culture in mung bean broth (15 g mung bean boiled in 1 L of ddH_2O for 20 min) at 26 °C with shaking at 200 rpm for 3 d. The concentration of fungal spores was determined using a hemocytometer, and the inoculum was calibrated to a concentration of 3×10^6 spores/mL [46]. Three-week-old watermelon plants were pretreated with different treatments, including ionic Fe, SA (99% purity; a positive control), bio-FeNPs, and SINCs, or ddH_2O (a negative control), by adding 50 mL suspension in ddH_2O of each treatment at 100 μg/mL concentration per pot with 3 plants. For disease assays, each treatment had five replicates. The pretreated plants were inoculated with *Fon* at 4 d post-treatment using the root dip method as described previously [47]. Briefly, the roots of the plants were dipped in the *Fon* spore suspension for 15 min and then replanted in a sterile potting mix. After inoculation, the plants were covered with polythene films to maintain infection conducive environment. The disease severity was recorded at 21 d post-inoculation (dpi) using a previously reported 4-scale rating standard [46].

To estimate invasive fungal growth, watermelon plants were hydroponically grown in *Fon* spore suspensions (3×10^6 spores/mL) amended with the above-mentioned treatments under shaking conditions at 95 rpm and 26 °C for a 9 d period [48]. Relative fungal growth was estimated using quantitative (q)PCR and expressed as a ratio of *FonOpm12* to *ClRps10* [47]. The *in vitro* antifungal potential was examined as described previously [37]. Briefly, mycelial plugs (5 mm in diameter) of a 4-d-old *Fon* culture were inoculated on potato dextrose agar plates supplied with ddH_2O (CK) and different above-indicated treatments at 100 μg/mL concentration, followed by the measurement of the radial growth diameter at 9 d post-incubation at 26 °C.

Microscopic observations

The morphology and cellular features of NPs-treated and untreated healthy and *Fon*-infected roots were examined using SEM and TEM, following previously described protocols [37]. Briefly, healthy or infected watermelon roots were incubated with or without bio-FeNPs and SINCs (100 μg/mL) at 26 °C with shaking at 95 rpm for 1 d. The root tips were incised, cleansed three times with phosphate buffer saline (100 mM and pH 7), and then prepared for observations under SEM and TEM. Six samples from each treatment group were subjected to SEM/TEM analysis, and minimum 5 fields were examined per sample.

RNA extraction and reverse transcriptase-qPCR analysis

Total RNA was extracted using the standard protocol of Trizol reagent (Vazyme Biotech, Nanjing, China), followed by cDNA synthesis using HiScript II QRT SuperMix (Vazyme Biotech, Nanjing, China), following the provided instructions. AceQ qPCR SYBR Green Master Mix (Vazyme Biotech, Nanjing, China) was used to prepare qPCR reactions, which were run with three technical replicates on a qPCR system (Roche LightCycler 96, Indianapolis, IN, USA). *ClTUA* was used for normalizing expression data. The relative transcript abundance of the target genes was calculated using the $2^{-\Delta\Delta CT}$ method [49]. The primers used are listed in Table S1.

Data analysis

The experiments were independently performed three times, and the results are shown as the average ± standard deviation (SD). The data from three independent experiments were analyzed using one-way analysis of variance (ANOVA) using the Statistix software v8.0. Fisher's least significant difference test was employed to determine the statistical significance between treatment means at a p-value ≤ 0.05 [50].

Results and discussion

Isolation and molecular characterization of B. marisflavi ZJ-4

A total of 9 morphologically distinct bacterial isolates were obtained, and strain ZJ-4 exhibited the highest tolerance level (8 mM) against $FeSO_4{\cdot}7H_2O$ (Fig. 1a, and Table S2). BLASTn-based sequence similarity searching indicated that the *16S rRNA* gene sequence of the strain ZJ-4 (accession no. OQ407476) had 100% sequence similarity to *B. marisflavi* Lar22 (MN709263) and *B. marisflavi* MI12 (MN117688), while the *rpoB* gene sequence (accession no. OQ411629) exhibited 100% sequence identity to *B. marisflavi* 151–25 (CP047095) and *B. marisflavi* F17 (CP085398). In the phylogenetic trees of the *16S rRNA* and *rpoB* genes, the strain ZJ-4 was grouped with *B. marisflavi* Lar22 (MN709263) and *B. marisflavi* 151–25 (CP047095), respectively (Fig. 1b and c). These results indicate the taxonomic identity of the ZJ-4 strain as *B. marisflavi*.

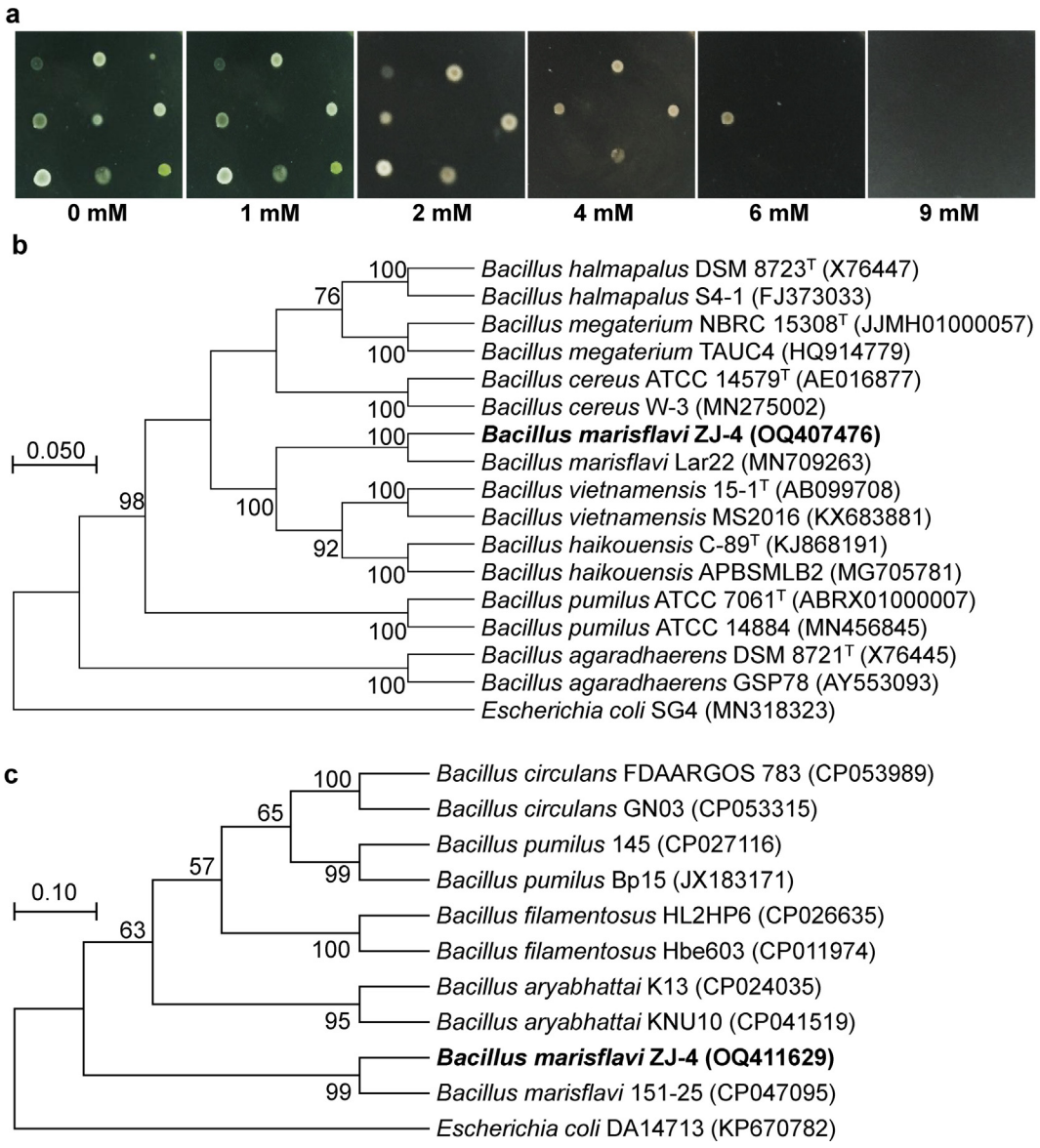

Fig. 1. Screening of Fe-resistant bacterial isolates and taxonomic characterization of *B. marisflavi* ZJ-4. (a) Minimum inhibitory concentrations of different isolates grown on nutrient agar plates amended with $FeSO_4{\cdot}7H_2O$ for 24 h at 28 °C. (b) A phylogenetic tree of *16S rRNA* gene and (c) a phylogenetic tree of *rpoB* gene of *B. marisflavi* ZJ-4 with other *Bacillus* species. Phylogenetic trees were constructed using the Maximum Likelihood method. Evolutionary distances were inferred using Maximum Composite Likelihood model using 1000-bootstrap repeats. Bootstrap values (≥50%) are shown at each branch point. *Escherichia coli* SG4 (MN318323) and *Escherichia coli* DA14713 (KP670782) were used as outgroups for *16S rRNA* and *rpoB* genes, respectively.

Production and physio-chemical properties of bio-FeNPs and SINCs

Extracellular biosynthesis of metallic NPs using culture supernatants of *Bacillus* spp. has been widely reported [5,51]. In the present study, bio-FeNPs were extracellularly synthesized using cell-free supernatant of *B. marisflavi* ZJ-4 with $FeSO_4{\cdot}7H_2O$ as starting materials. UV–vis spectroscopy results confirmed the successful synthesis of bio-FeNPs. The UV–vis spectra showed a strong absorption peak around 305.59 nm (Fig. S1), indicating the presence of Fe-based NPs in the reaction mixture. Furthermore, the spectra also showed an additional minor peak at 230 nm, a typical characteristic of metal NPs with small size [52]. These features are consistent with previous studies that synthesized magnetic FeNPs from the culture supernatants of *B. aryabhattai* RNT7 and *Bacillus cereus* HMH1 [5,53]. Previous studies have suggested that cell-free extract from *Bacillus* species possesses strong reduction potential, converting ionic substrate into stabilized NPs [54,55]. Overall, these results confirm the reduction potential of biomolecules in the cell-free filtrate of *B. marisflavi* ZJ-4 to produce FeNPs from $FeSO_4{\cdot}7H_2O$.

During NPs biosynthesis, different extracellular biomolecules have been reported to stabilize and coat metallic NPs surface [56]. For example, various extracellular metabolites of *Bacillus megaterium* NOM14, such as alcoholic, carboxylic, and organic compounds, were previously shown to stabilize bio-manganese NPs [37]. Similarly, in the present study, FTIR analysis indicated the presence of the various functional groups in bio-FeNPs, such as O–H stretching vibrations in the range of 3386 cm^{-1}, C = C stretching vibrations at 1648 cm^{-1}, O–H bending vibrations at 1406 cm^{-1}, and C-N stretching vibrations at 1054 cm^{-1} (Fig. 2a), implying the presence of organic compounds, including alcohols, alkenes, and amines. However, the FTIR spectra of SINCs showed characteristic peaks at 3422 cm^{-1}, 1,630 cm^{-1}, 1076 cm^{-1}, 888 cm^{-1}, and 577 cm^{-1}, which were attributed to O–H stretching

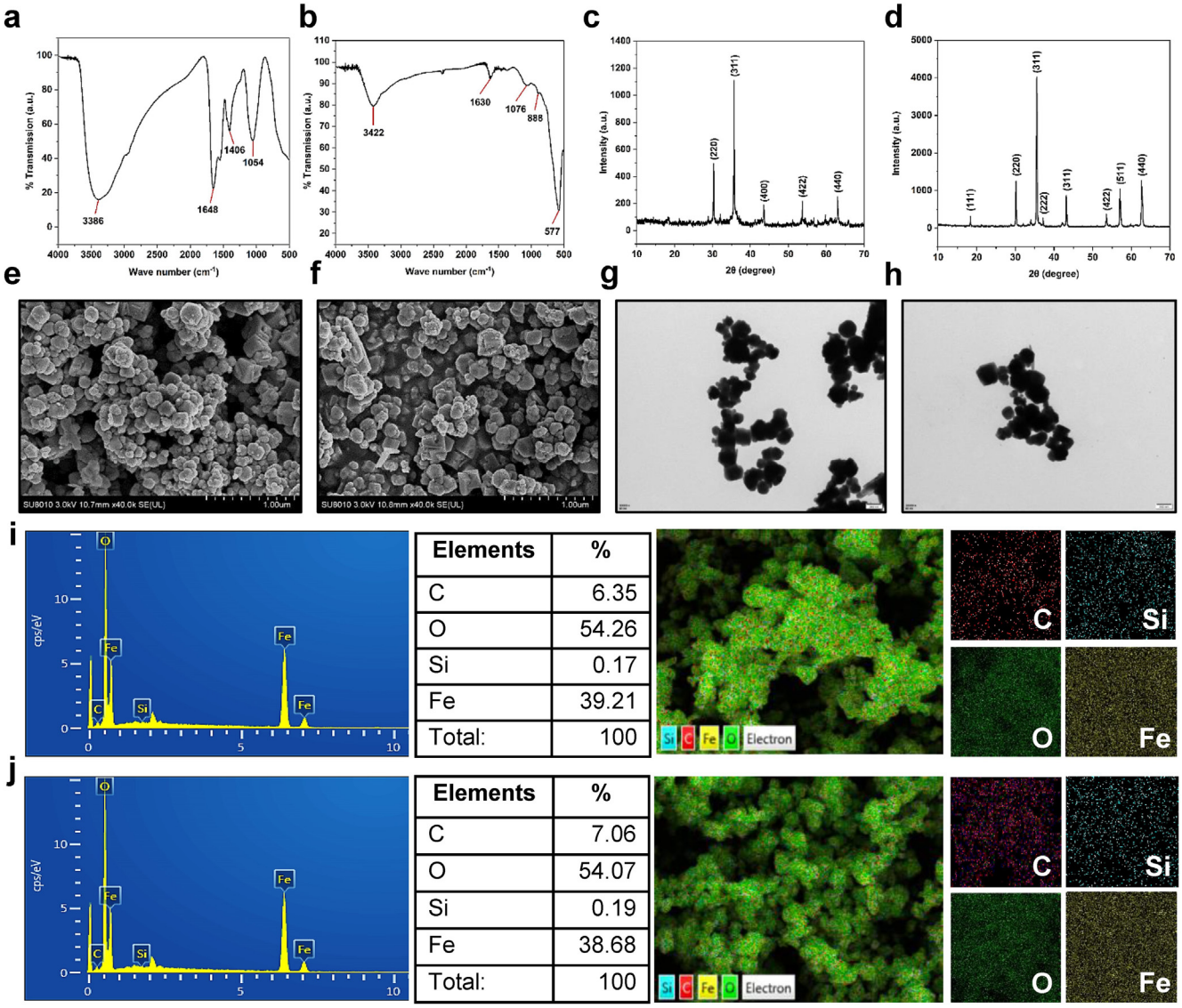

Fig. 2. Physico-morphological properties of bio-FeNPs and SINCs. FTIR spectra indicating the presence of different functional groups around the surface of (a) bio-FeNPs and (b) SINCs. XRD spectra revealing the crystalline phase of (c) bio-FeNPs and (d) SINCs. SEM images showing the morphology of (e) bio-FeNPs and (f) SINCs. Size distribution of bio-FeNPs and SINCs was calculated from SEM micrographs using ImageJ software. TEM images showing shapes and structure of (g) bio-FeNPs and (h) SINCs in dissolved form. EDS spectra (*left*) and elemental mapping (*right*) showing chemical composition and fractions of (i) bio-FeNPs and (j) SINCs. The most abundant elements are displayed by fluorescence: C - red; O - green; Si - blue; Fe - yellow. (For interpretation of the references to color in this figure legend, the reader is referred to the web version of this article.)

of alcohols, C = N stretching of oximes, C-N stretching of amines, C = C bending of alkenes, and C-I stretching of halo compounds, respectively (Fig. 2b). Similarly, the presence of alcoholic, carboxylic, and organic functional groups as surface coatings of bio-FeNPs has been previously reported [5]. Collectively, the FTIR analysis confirms the presence of various functional groups in bio-FeNPs and SINCs, providing insights into the chemical composition of the synthesized NPs, and successful synthesis of NPs with hydroxyl/organic functional groups present in ZJ-4 culture filtrate. These results align with previous findings that identified similar alcoholic and organic functional groups secreted by *Bacillus altitudinis* WM-2/2 for stabilizing bio-copper NPs [55].

The crystalline features of synthesized NPs were obtained using XRD analysis. The XRD spectra of bio-FeNPs showed characteristic peaks at 2θ values of 30.8°, 36.2°, 43°, 53.9°, and 63.1°, which were assigned to the (220), (311), (400), (422), and (440) crystal planes of the cubic phase of Fe, respectively (Fig. 2c). These crystalline features are of great significance as they provide valuable insights into the physical state, release kinetics, and interaction capacity of NPs with the encapsulating substrate. Similarly, SINCs showed that diffraction peaks observed at 2θ values of 18.4°, 30.8°, 36.2°, 38.5°, 43°, 53.9°, 57.6°, and 63.1° corresponded to (111), (220), (311), (222), (311), (422), (511), and (440) (Fig. 2d). These data confirmed that the synthesized bio-FeNPs and SINCs were crystalline in nature and had a cubic phase, which is consistent with previous study results [5,31,57]. The XRD results indicate the high quality and homogeneity of the synthesized NPs. SEM images of bio-FeNPs and SINCs showed the presence of aggregated NPs with irregular shapes and average particle sizes of ~72.35 nm and ~65.87 nm, respectively (Fig. 2e and f). TEM images further confirmed the aggregation of the particles in bio-FeNPs and SINCs, revealing the clusters of particles (Fig. 2g and h). The aggregates were found to have a dense and homogeneous structure, indicating the stability of the NPs, which is similar to

previous findings reporting the production of stabilized aggregates of manganese and copper NPs by bacterial culture filtrates [37,39]. The SEM and TEM results demonstrate the formation of aggregated NPs (Fig. 2e-h), suggesting the need for further optimization of the synthesis conditions to obtain monodispersed NPs. These findings corroborate with previous results reporting the extracellular production of aggregated copper NPs [55,58]. The aggregation might be due to the strong tendency of particles to stick together. The results of the EDS analysis of FeNPs and SINCs showed their elemental composition. The EDS spectra of FeNPs and SINCs showed the presence of elements, including Carbon (C), Oxygen (O), Silicon (Si), and Iron (Fe). The relative abundance of each atomic fraction in FeNPs and SINCs was calculated at a specific position of the NPs, and it was observed that O constituted the major component (54.26% and 54.07%, respectively), followed by Fe (39.21% and 38.68%, respectively), C (6.35% and 7.06%, respectively), and Si (0.17% and 0.19%, respectively) (Fig. 2i and j). The characterization data confirm the successful production of biomolecules-stabilized bio-FeNPs and SINCs with variable morphology.

Stoichiometric chemical fractions and stability of bio-FeNPs and SINCs

We absorptiometrically determined the levels of SA and Fe in 100 μg of SINCs relative to the same weight of purified SA and bio-FeNPs (Fig. S2a). The absorption spectra of 100 μg/mL of SINCs showed a lower but insignificant level of SA than that in purified SA powder, showing absorption values of 7.12 ± 0.30 and 8.15 ± 0.63, respectively, at 296 nm (Fig. S2a). Similarly, absorption spectra of bio-FeNPs and SINCs revealed that 100 μg/mL of SINCs contained less but statistically insignificant amount of Fe than that in bio-FeNPs (Fig. S2a). Similar absorption spectra were observed for chemical-based acetyl-SA-coated copper oxide NCs [59]. Collectively, these results indicate that SINCs have nearly identical chemical fractions as in the source compounds.

The dissolution of bio-FeNPs and SINCs in ddH_2O and potting mix was evaluated to assess their stability, efficacy, and metal ions release rate. The results of the dissolution assays in ddH_2O and potting mix showed that the release of Fe ions from the bio-FeNPs and SINCs was gradual over different time intervals, showing the maximum release at 24 h in both ddH_2O (1.86 μg/mL and 1.53 μg/mL, respectively) and potting mix (2.39 μg/mL and 1.81 μg/mL, respectively) (Fig. S2b). The slow metal release rate of SINCs indicated their better stability and integrity in the medium than bio-FeNPs. Moreover, the concentration of the dissolved Fe from bio-FeNPs and SINCs was found to be higher (22% and 15%, respectively) in potting mix compared to the ddH_2O at 24 h (Fig. S2b). This metal release profile of biosynthesized NPs is of great significance, specifically in the potting mix extract that mimics real agriculture conditions, providing comprehensive insights into the active ingredient release behavior and functional stability/integrity of bio-FeNPs and SINCs. These results coincide with a recent study, showing a similar metal release profile for bio-chitosan-FeNCs in phosphate buffer [5]. Overall, these results provide valuable insights into the bioavailability of Fe ions from bio-FeNPs and SINCs in different environments, indicating that these NPs can serve as carriers for Fe ions in neutral to acidic soils.

Growth promotion of watermelon plants by bio-FeNPs and SINCs

The growth-promoting effects of exogenously applied FeNPs and SA on watermelon plants have been previously reported [60,61]. However, variable impacts of exogenous SA on plant growth have been reported previously, with some studies indicating an inhibitory effect at a higher concentration of 100 mM, while others showing a beneficial impact at a lower concentration of 0.3∼0.4 mM [62,63]. Thus, we examined the growth performance of watermelon plants treated with bio-FeNPs and SINCs and found a significant improvement in their agronomic traits compared to the untreated and treated controls, with the SINCs supplementation showing a higher increase in the growth parameters compared to the untreated, ionic Fe-, and SA-treated controls (Fig. 3a). The plants grown with bio-FeNPs and SINCs showed an increase in plant height (20% and 32%, respectively), fresh weight (32% and 43%, respectively), and dry weight (42% and 49%, respectively) compared to the untreated plants (Fig. 3b), which correlate with previous results demonstrating the improvement of growth and development in bio-FeNPs-treated mung bean plants [64]. In another study, the chitosan-coated zinc oxide NCs-treated pepper plants showed enhanced growth and biomass compared to bare zinc oxide NPs-treated plants [65]. Similarly, plants treated with ionic Fe significantly enhanced the fresh weight (12%), while plants with SA showed a significant increment in plant fresh weight (29%) and dry weight (39%) as compared to the untreated plants (Fig. 3c and d). The greater improvement in the growth attributes of SINCs-treated watermelon plants was due to the cumulative effect of nanoscale Fe and SA [66,67]. These results suggest that the Fe-based NPs supplementation, specifically SINCs treatment, improves the agronomic traits of the watermelon plants, which can positively impact their overall growth and productivity.

The Fe content analysis revealed a significant increment in Fe concentration in roots and stems of the watermelon plants exposed to bio-FeNPs and SINCs compared to the untreated, ionic Fe-, and SA-treated control groups (Fig. 3e). The plants treated with bio-FeNPs showed an average increase of 21% in Fe content in roots and 65% in stems, while the SINCs-treated plants showed even a higher increase of 24% in Fe content in roots and 67% in stems compared to untreated controls, which was statistically insignificant to bio-FeNPs treatment (Fig. 3e). These results indicate that both bio-FeNPs and SINCs can effectively enhance Fe uptake by watermelon plants. The TF, which measures the Fe translocation from roots to stems, was found to be 56% higher in bio-FeNPs- and SINCs-treated plants compared to the untreated, ionic Fe-, and SA-treated control plants; however, ionic Fe and SA did not show notable impact on the Fe uptake and translocation in plant tissues than untreated controls (Fig. 3f). The better Fe content in plant tissues exposed to nanoscale Fe might be due to its unique properties and higher biocompatibilities as compared to chemical counterparts [68]. Moreover, higher bioavailability of Fe ions from FeNPs and SINCs resulted in better *in planta* Fe accumulation [5]. These findings suggest that applying bio-FeNPs and SINCs can provide an alternative way of enhancing Fe nutrition in crops to improve plant growth and productivity.

Suppression of watermelon Fusarium wilt by bio-FeNPs and SINCs

Although the disease suppression capability of chemical-based NPs against various phytopathogens has been reported [1,69–71], recent progress has been made to evaluate the disease-suppressive potential of bio-NPs and NCs [5,55]. For example, bio-copper NPs suppressed Fusarium wilt in musk melon by inducing SAR response through activating defense-related *PR* genes [72]. The disease-suppressive role of exogenously applied SA *via* inducing plant immunity against pathogen attack has been well-established [19,73]. However, the disease-suppressive role of SA-coated NCs remains to be established. In this study, the disease suppression capacity of bio-FeNPs and SINCs was evaluated and results showed that pretreatment of watermelon plants with bio-FeNPs and SINCs effectively suppressed the incidence of Fusarium wilt, with SINCs showing most prominent disease-suppressive potential compared to the untreated, ionic Fe-, and SA-treated infected plants (Fig. 4a). The disease severity was significantly lower in the plants primed with 100 μg/mL SA, bio-FeNPs, and

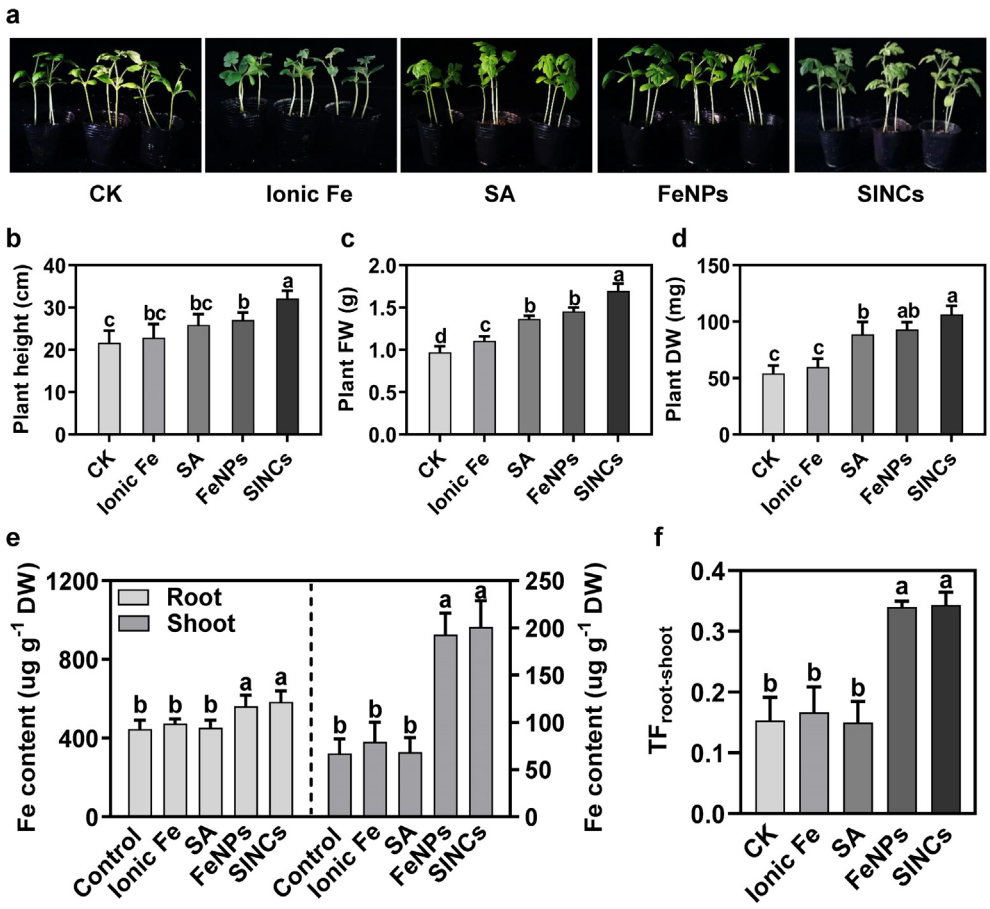

Fig. 3. Soil drenching with bio-FeNPs and SINCs improved the growth performance and Fe content of watermelon plants. (a) Growth phenotype of watermelon plants at 15 d post-treatment with ionic Fe, SA, bio-FeNPs, or SINCs. (b) Plant height, (c) fresh and (d) dry biomass at 15 d post-treatment with ionic Fe, SA, bio-FeNPs, or SINCs. (e) Fe content in roots (*left*) and shoots (*right*) of healthy plants at 15 d post-treatment with ionic Fe, SA, bio-FeNPs, or SINCs. (f) Fe distribution from root-to-shoot, measured in terms of $TF_{root\text{-}shoot}$, at 15 d post-treatment with ionic Fe, SA, bio-FeNPs, or SINCs. Data presented are the means ± SD from three independent experiments and different lowercase letters above the error bars represent the significant difference among different datasets inferred by one-way ANOVA at p-value ≤ 0.05.

SINCs compared to the untreated control plants, with an average reduction of 30%, 42%, and 59% in disease severity indices, respectively, compared to untreated diseased plants (Fig. 4b). The pretreatment of SA, bio-FeNPs, and SINCs significantly suppressed the appearance of disease symptoms in the *Fon*-inoculated plants, where 27%, 40%, and 53% of the infected plants showed no or mild disease symptoms, compared to ionic Fe-treated and untreated diseased plants (Fig. 4c). At 21 dpi, >70% of ionic Fe-supplied and unsupplied infected plants died, while the death rate of the SA-, bio-FeNPs-, and SINCs-pretreated infected plants was found to be 60%, 40%, and 13%, respectively (Fig. 4c). These results are in line with a recent study demonstrating that the soil-based application of green-synthesized FeNPs suppressed Fusarium wilt in tomato through direct pathogen inhibition and improving important physiological processes [11]. Similarly, bio-silver NPs have been shown to induce metabolic and antioxidative protective mechanisms to suppress Fusarium wilt in pepper [74]. Moreover, exogenous SA application has been shown to suppress Fusarium wilt in watermelon by triggering phytohormone-linked protective mechanisms and modulating the rhizobiome [24,25]. Thus, the better disease-suppressive capability of SINCs could be due to their high stability and slow release of active ingredients (Fig. S2), such as SA, Fe ions, and other coated biomolecules, contributing to the overall functionality of bio-NPs [58]. Collectively, these findings suggest that the application of Fe-based NPs as a soil drench, specifically SINCs, can be effective in controlling Fusarium wilt in watermelon.

The invasive fungal growth in host tissues is one of the key events of *Fon* infection on watermelon plants [75], leading to obstructed water supply, wilting, and ultimately plant death. To investigate the alterations in the infection behavior of *Fon* upon bio-FeNPs and SINCs exposure, *in planta* fungal growth in the root and stem tissues of diseased plants was analyzed. The results showed a significant reduction in *Fon* invasive fungal growth in watermelon roots (28%, 43%, and 53%) and stems (29%, 55%, and 69%) upon exposure to SA, bio-FeNPs, and SINCs, respectively, at 9 dpi compared to the untreated control plants (Fig. 4d and e). SINCs treatment was found to be the most effective, which resulted in a higher decrease of *Fon* invasive growth compared to the untreated, ionic Fe-, and SA-treated controls at each time interval (Fig. 4d and e), suggesting that reduction in the disease severity is linked to decreased pathogen invasion into watermelon tissues. Together with previous results demonstrating lower growth of *Fon* and *F. solani* in bio-MnNPs-treated watermelon and SA-treated soybean tissues, respectively [20,37], these findings highlight the potential of SINCs as an effective tool in mitigating Fusarium wilt development in watermelon by controlling invasive pathogen growth in plant tissues.

Direct antifungal activity of bio-NPs against plant pathogenic fungi has been well-established [54,76]. For example, bio-FeNPs have been reported to exhibit tremendous antifungal activity against *Aspergillus niger*, *F. oxysporum*, and *Sclerotinia sclerotiorum* [12,77]. Thus, we investigated the *in vitro* antifungal activity of

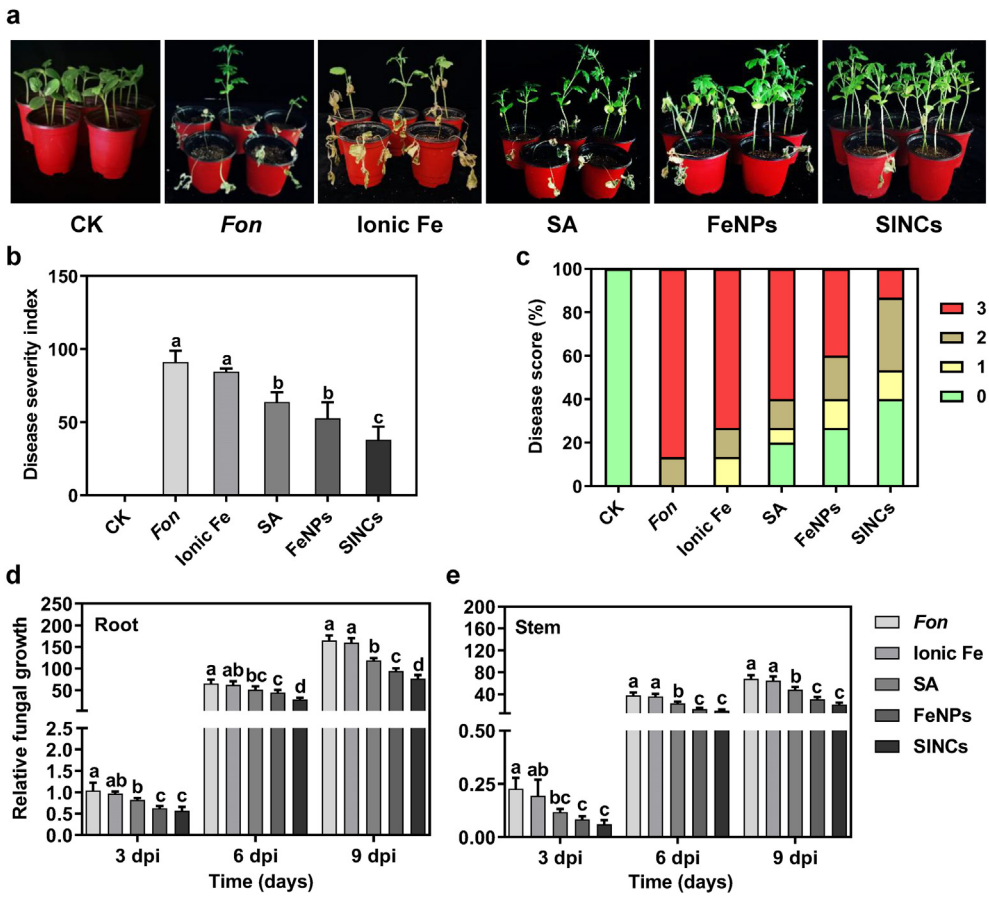

Fig. 4. Soil drenching with bio-FeNPs and SINCs suppressed watermelon Fusarium wilt. (a) Phenotype of diseased plants primed with ddH_2O (CK), ionic Fe, SA, bio-FeNPs, or SINCs at 21 dpi. (b) Disease severity indices and (c) disease ratings of the *Fon*-inoculated plants primed with ddH_2O (CK), ionic Fe, SA, bio-FeNPs, or SINCs at 21 dpi. Two-week-old plants were pretreated with ddH_2O (CK), ionic Fe, SA, bio-FeNPs, or SINCs by soil drenching and root-inoculated at 4 d post-treatment. Disease scores were recorded by a 4-scale rating standard. Fungal growth in (d) roots and (e) stems of *Fon*-inoculated plants treated with ionic Fe, SA, bio-FeNPs, or SINCs at 3, 6, and 9 dpi. Two-week-old plants were hydroponically grown in *Fon* spore suspension amended with indicated treatments under shaking conditions. Relative fungal biomass was represented as a ratio of transcript level *FonOpm12* to *ClRps10*, which was measured using qPCR. Experiments with five biological repeats (n = 5) were repeated independently three times with similar results. Data presented are the means ± SD from three independent experiments and different lowercase letters above the error bars represent the significant difference among different datasets inferred by one-way ANOVA at p-value ≤ 0.05.

bio-FeNPs and SINCs against *Fon* to uncover the basis for the reduced fungal invasive growth within watermelon tissues. Surprisingly, bio-FeNPs and SINCs did not show any inhibitory impact on the mycelial growth of *Fon* (Fig. S3). It is, therefore, unlikely that the reduced fungal invasive growth was due to the direct antifungal activity of bio-FeNPs and SINCs against *Fon*. Notably, the lower *in planta* growth of *Fon* in SINCs-pretreated watermelon plants could be due to increased endogenous SA level, which is similar to previous observations in *F. solani*-infected soybean plants [20].

Oxidative homeostasis system modulation by bio-FeNPs and SINCs

The results of the physiological and biochemical assays showed a significant reduction in the levels of H_2O_2, $O_2^{\bullet-}$, and MDA, the most common indicators of oxidative stress, in roots and stem tissues of healthy watermelon plants upon SA, bio-FeNPs, and SINCs exposure than ionic Fe-treated and untreated plants (Fig. 5a-c). The data showed that H_2O_2 production was reduced in roots (41%, 54%, and 72%) and stems (37%, 44%, and 59%) of SA-, bio-FeNPs-, and SINCs-treated plants, respectively, compared to untreated healthy plants (Fig. 5a). Similarly, $O_2^{\bullet-}$ levels were lowered in roots (14%, 29%, and 45%) and stems (17%, 30%, and 46%) of SA-, FeNPs-, and SINCs-treated plants, respectively, than untreated healthy controls (Fig. 5b). Further, the application of SA and bio-FeNPs reduced MDA levels in roots (46% and 53%, respectively) and stems (22% and 37%, respectively) compared to the healthy controls (Fig. 5c). The most significant reduction in MDA level, however, was observed in the SINCs-treated plants than the untreated, ionic Fe-, SA- and bio-FeNPs-treated plants, with an average decrease of 78% in roots and 52% in stems compared to untreated plants (Fig. 5c). Furthermore, the treatment with SA, bio-FeNPs, and SINCs led to a notable increase in enzymatic antioxidants, including CAT, POD and SOD, in roots and stems of healthy watermelon plants than ionic Fe-treated and untreated healthy plants (Fig. 5d-f). The highest levels of CAT, POD, and SOD were recorded in the samples treated with SINCs compared to the untreated, ionic Fe-, and SA-treated controls (Fig. 5d-f). For example, CAT activity was increased by 69% in the roots and 62% in the stems (Fig. 5d), while POD level was increased by 58% in the roots and 63% in the stems in response to SINCs treatment (Fig. 5e). Furthermore, SOD activity was increased by 68% in the roots and 62% in the stems (Fig. 5f). Similarly, it has been reported that chitosan-coated zinc oxide NPs improved physiological profile by promoting enzymatic antioxidants, including CAT and POD, in pepper [65]. In another study, SA treatment at 0.5 mM level improved the antioxidative capacity in tomato plants [78], indicating that better oxidative balance of SINCs-treated watermelon plants was due to the synergistic impact of SINCs-released Fe and SA in inducing antioxidative

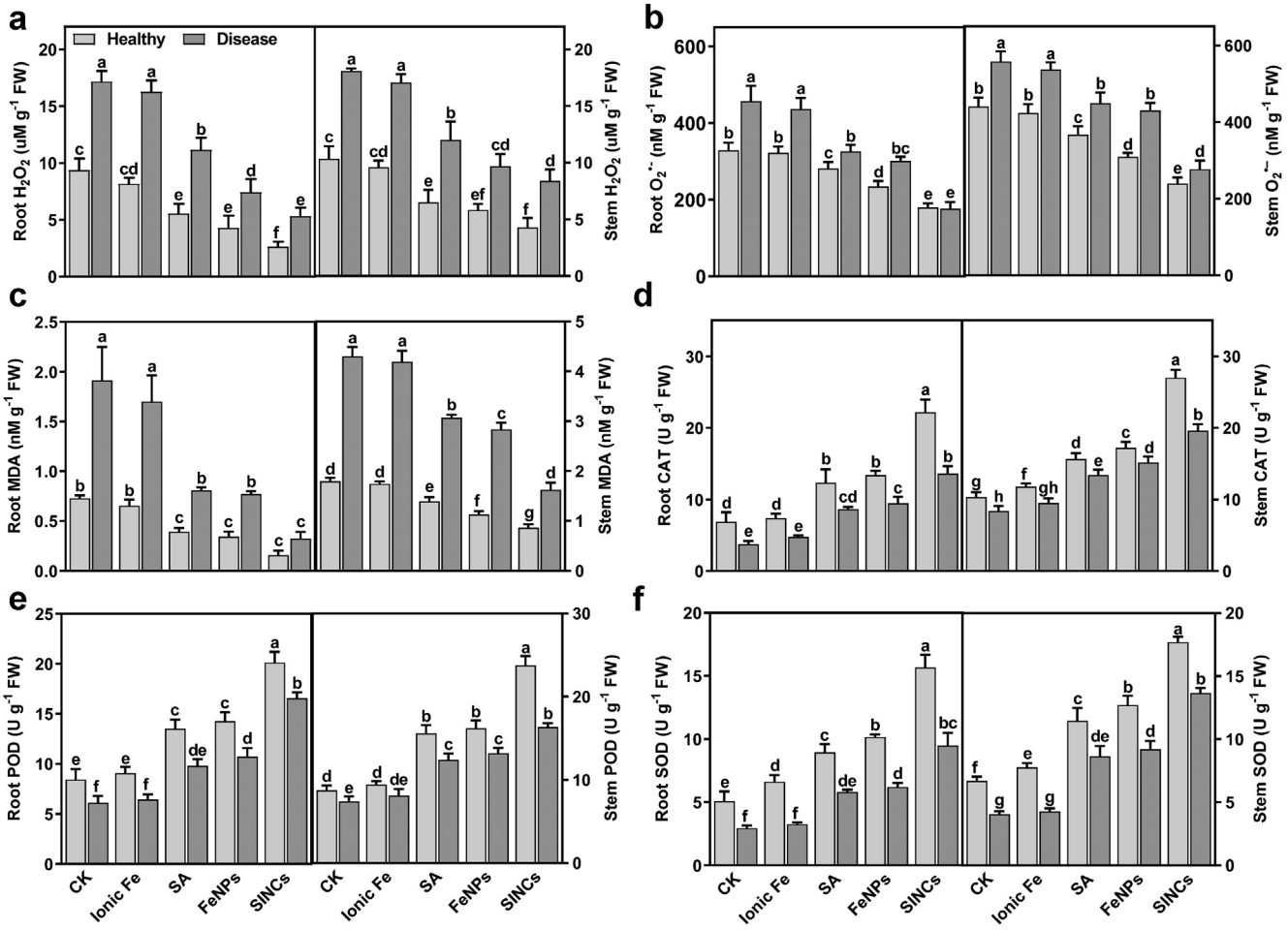

Fig. 5. Soil drenching with bio-FeNPs and SINCs modulated ROS balancing system in healthy and diseased watermelon plants. (a) H_2O_2 level, (b) $O_2^{\bullet-}$ generation, and (c) MDA content in roots and stems of plants treated with ddH_2O (CK), ionic Fe, SA, bio-FeNPs, or SINCs. (d) CAT, (e) POD, and (f) SOD activities in roots and stems of plants treated with ddH_2O (CK), ionic Fe, SA, bio-FeNPs, or SINCs. Data presented are the means ± SD from three independent experiments and different lowercase letters above the column represent the significant difference among different datasets inferred by one-way ANOVA at p-value ≤ 0.05.

machinery. The observed biological effects (Figs. 4-5) provide valuable insights into the enhanced efficacy of FeNPs and SINCs compared to Fe and SA. Further, it has been widely reported that the unique properties of NPs, such as enhanced biocompatibility and uptake (Fig. 3e and f), can result in different biological responses compared to their chemical counterparts [1,3,55], supporting the notion that low amounts of NPs can exhibit superior effects compared to higher/similar concentrations of their bulk or ionic form.

In diseased plants, application of SA, bio-FeNPs, and most prominently SINCs resulted in a significant reduction of ROS accumulation *via* boosting enzymatic antioxidants compared to the untreated, ionic Fe-, and SA-treated diseased plants (Fig. 5). The data showed that H_2O_2 production was reduced in roots (35%, 57%, and 69%) and stems (34%, 46%, and 54%) of the SA-, bio-FeNPs-, and SINCs-treated plants, respectively, compared to the untreated disease controls (Fig. 5a). Similarly, $O_2^{\bullet-}$ levels were decreased in roots (29%, 34%, and 61%) and stems (19%, 23%, and 50%) of the SA-, FeNPs-, and SINCs-treated plants, respectively, compared to the untreated infected controls (Fig. 5b). Further, the application of SA and FeNPs reduced MDA levels in roots (58% and 60%, respectively) and stems (29% and 34%, respectively) compared to the diseased controls (Fig. 5c). The most significant reduction in MDA level, however, was observed in the SINCs-treated plants as compared to the untreated, ionic Fe-, and SA-treated diseased plants, with a decrease of 83% in roots and 62% in stems than untreated infected plants (Fig. 5c). Furthermore, the treatment with SA, bio-FeNPs, and SINCs led to a notable increase in enzymatic antioxidants, including CAT, POD and SOD, in roots and stems of diseased watermelon plants than ionic Fe-treated and untreated healthy plants (Fig. 5d-f). Compared to other treatments, the highest levels of CAT, POD, and SOD were recorded in the samples treated with SINCs. For example, CAT activity was increased by 72% in the roots and 57% in the stems (Fig. 5d), while POD level was increased by 63% in the roots and 55% in the stems in response to SINCs treatment (Fig. 5e). Furthermore, SOD activity was increased by 69% in the roots and 70% in the stems (Fig. 5f). However, the diseased watermelon plants treated with ionic Fe did not show any remarkable impact on the studied physiological features (Fig. 5), indicating that the positive impact of synthesized NPs on the physiological processes of watermelon plants is strongly linked to their unique properties, including small size, greater biocompatibility, surface properties, and capping biomolecules. These results coincide with a previous study reporting that bio-FeNPs suppressed Fusarium wilt in tomato by scavenging ROS generation through activating enzymatic antioxidants [79]. Similarly, exogenously applied 200 μM SA as a soil drench activated enzymatic antioxidants, such as POD, to mitigate oxidative stress and suppress Fusarium wilt in tomato [80], corroborating the fact that SA activates SAR against phytopathogens by manipulating redox signaling pathways [81]. Overall, these results suggest

that SINCs have a greater antioxidant potential than SA and FeNPs, and thus can play a key role in maintaining the oxidative balance of the watermelon plants. The fact that the SINCs-treated plants showed the lowest level of ROS and highest antioxidative enzyme activities upon *Fon* infection demonstrates that SINCs can effectively alleviate the *Fon*-triggered oxidative stress damage in watermelon plants. Based on the better growth-promoting and disease-controlling potential under greenhouse conditions, bio-FeNPs, and SINCs were selected to study disease-suppressive mechanisms further.

NPs-Fon interaction on the watermelon root surface and subcellular space

We further examined the direct interaction of *Fon* with FeNPs and SINCs on the root surface and within the root tissue. SEM images showed that roots treated with 100 μg/mL bio-FeNPs and SINCs maintained normal morphology (Fig. 6a), and elemental composition through SEM-EDS analysis showed the specific elemental composition of Fe on the root surfaces treated with FeNPs and SINCs (Fig. S4). Conversely, the normal root surface was disrupted upon *Fon* infection, with fungal hyphae penetrated the root surface, while the application of bio-FeNPs and SINCs rescued morphological defects induced by hyphal penetration in the root tissues of infected plants (Fig. 6a). SINCs was found to be the most effective treatment, showing notably less hyphal penetration and intact root surface (Fig. 6a). Similarly, copper NPs have been shown to protect *Fusarium virguliforme*-induced morphological damages in soybean plants *via* forming a protective sheet over the plant surface to limit pathogen invasion [70]. Additionally, a higher presence of elemental Fe was evident on the root surface of bio-FeNPs- and SINCs-treated diseased plants than the untreated infected plants (Fig. S4). These findings provide insights into direct interactions between bio-NPs/NCs and *Fon* on plant root surface.

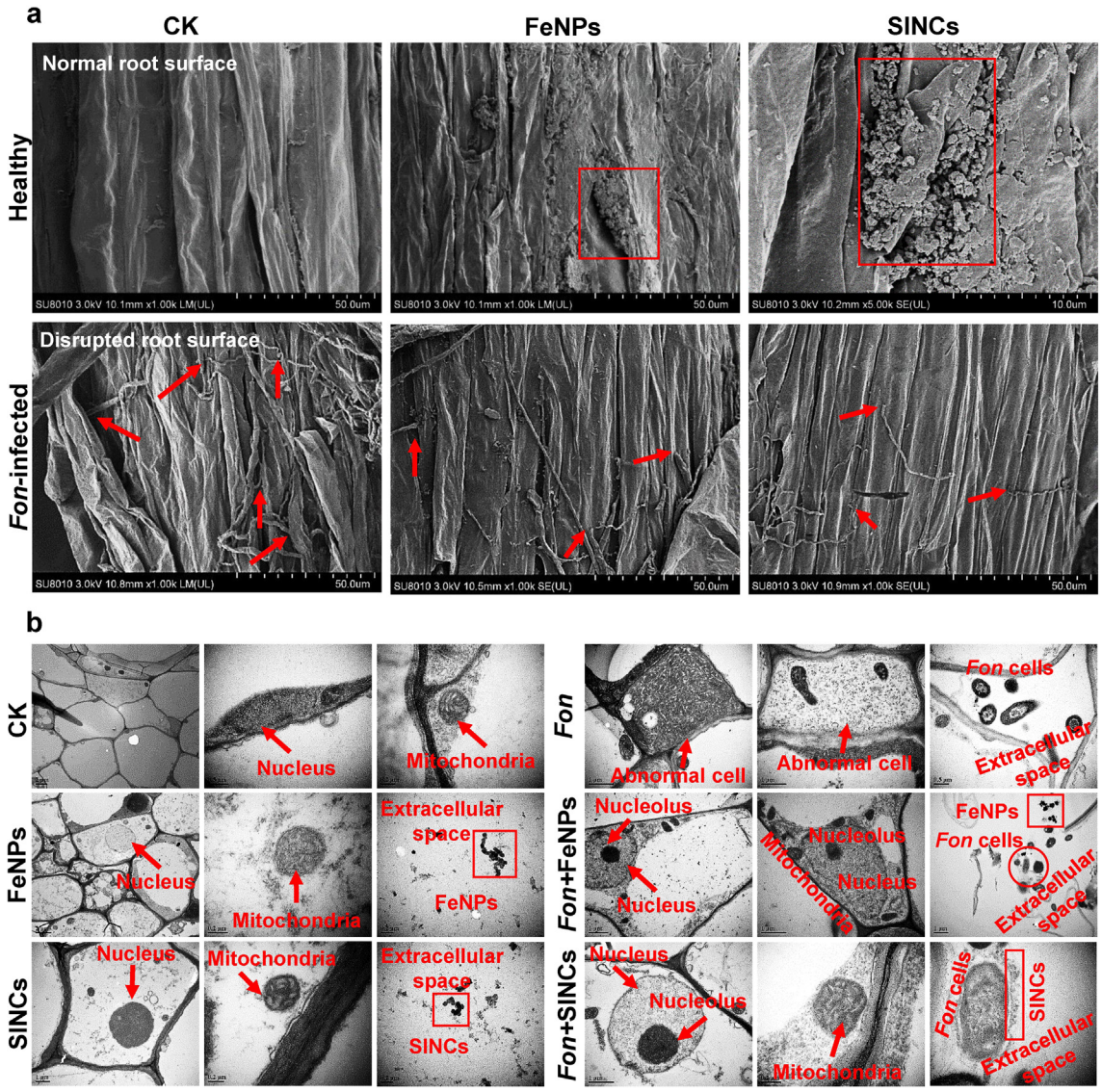

Fig. 6. Distribution and interaction of bio-FeNPs and SINCs with the root tissues of healthy and *Fon*-infected watermelon plants. (a) SEM images showing morphological phenotype of roots of mock-inoculated (*upper*) and *Fon*-inoculated plants (*lower*) treated with ddH_2O (CK), bio-FeNPs, or SINCs. Red boxes indicate accumulation of FeNPs or SINCs on the root surface, while arrows indicate the invading and restricted hyphae of *Fon* on the root surface in SEM micrograph. (b) TEM images showing ultrastructural changes in root cells of mock-inoculated (*left*) and *Fon*-inoculated plants (*right*) treated with ddH_2O (CK), bio-FeNPs, or SINCs. Subcellular structures and organelles are labelled in red text, while accumulation of *Fon* and NPs are indicated in red circle and boxes, respectively. Experiments were repeated independently three times with similar results and data from one representative experiment is shown. (For interpretation of the references to color in this figure legend, the reader is referred to the web version of this article.)

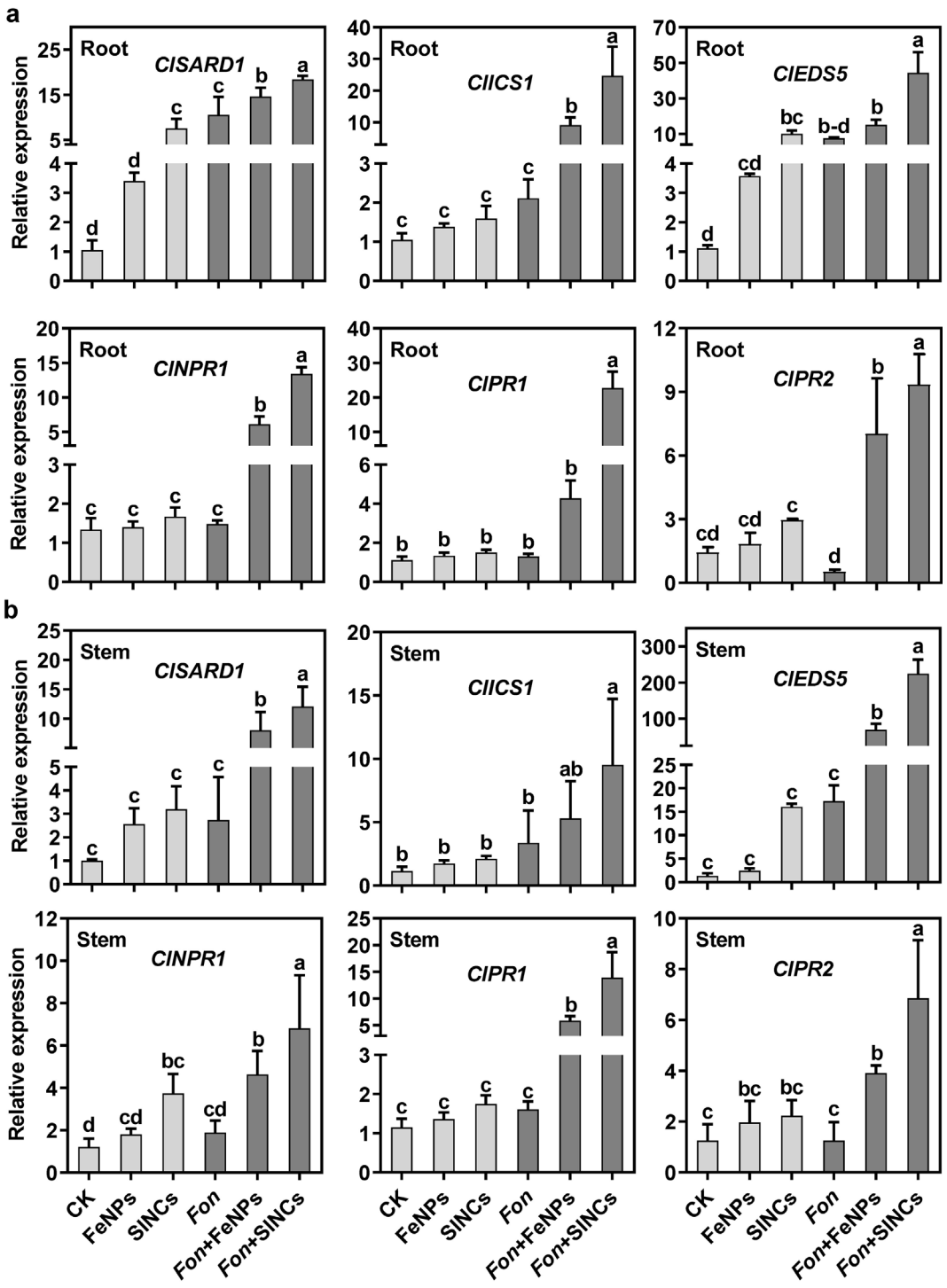

Fig. 7. Application of bio-FeNPs and SINCs triggered SA-dependent defense mechanism in healthy and disease watermelon plants. Expression of SA biosynthesis, signaling, and responsive genes in (a) roots and (b) stems of the mock-inoculated and *Fon*-inoculated plants pretreated with ddH_2O (CK), bio-FeNPs, or SINCs at 6 dpi. Data presented are the means ± SD from three independent experiments and different lowercase letters above the column represent the significant difference among different datasets inferred by one-way ANOVA at p-value ≤ 0.05.

To study the ultrastructural organization, TEM analysis was performed on healthy and *Fon*-infected watermelon roots exposed to bio-FeNPs and SINCs. The TEM images revealed a clear difference in the morphology of the root tissues between the healthy and infected plants (Fig. 6b). In healthy plants, the root tissues showed organized structures, including cellular membranes, nucleus and mitochondria, with well-defined cells, while the root tissues of the *Fon*-infected plants showed signs of damage and disorganization (Fig. 6b). Upon exposure to bio-FeNPs and SINCs, the healthy root tissues displayed organized structures, such as nucleus and mitochondria, with NPs accumulation in extracellular space, whereas the infected root tissues showed a noticeable improvement in their cellular structures and fewer signs of damage (Fig. 6b). These findings corroborate the positive impact of bio-FeNPs and SINCs in rescuing pathogen-induced morphological damages in infected root tissues and correlate with previous

results describing the shielding effect of bio-MnNPs against *Fon*-induced morphological damages in roots of infected watermelon plants [37]. In another recent study, bio-chitosan-Fe NCs shielded pathogen-induced ultrastructural damages in rice plants by accumulating within plant tissues [5]. The SEM and TEM results demonstrate that bio-FeNPs and SINCs positively affect the overall health of the roots, especially in infected plants, indicating a potential role in alleviating Fusarium wilt *via* restricting *Fon* invasion in root cells.

Activation of the SA-dependent defense response by bio-FeNPs and SINCs

It has recently been established that bio-NPs/NCs can trigger the expression of SA-responsive genes to suppress plant diseases [5,37]. Similarly, exogenous SA-mediated suppression of sudden death syndrome, caused by *F. solani*, in soybean has been reported to be linked with the activation of *GmSID2*, *GmNPR1*, *GmPR1*, and *GmEDS5* [20,82]. To elucidate the molecular mechanism of the bio-FeNPs- and SINCs-mediated Fusarium wilt suppression, the expression levels of *ClSARD1*, *ClICS1*, and *ClEDS5* (SA biosynthesis), *ClNPR1* (SA signaling), and *ClPR1* and *ClPR2* (SA responsive) genes were analyzed in roots and stems of healthy and infected watermelon plants exposed to bio-FeNPs and SINCs (Fig. 7). The exposure to SINCs resulted in the significantly highest expression of *ClSARD1* in healthy roots and *ClNPR1* in healthy stems compared to untreated healthy plants (Fig. 7a and b). Similar to SINCs treatment in healthy plants, *Fon* infection significantly induced the expression of *ClSARD1* in roots compared to healthy controls (Fig. 7a), which might not be strong enough to initiate a downstream defense response. Conversely, infected roots and stems showed significantly upregulated expression of all SA biosynthesis and responsive genes upon exposure to FeNPs (except *ClEDS5* in roots and *ClICS1* in stems) and SINCs compared to the untreated infected plants (Fig. 7a and b). Overall, SINCs have a better effect on the plant defense mechanisms than bio-FeNPs, indicating a link of the better SA accumulation in plant tissues to the SAR establishment by activating the expression of the SA biosynthesis, signaling, and responsive genes [81]. These results conform previous findings indicating that bio-Fe oxide and sulfur NPs suppressed Fusarium wilt in tomato *via* inducing *PR* genes-dependent SAR response [11,68]. Similarly, the immunomodulatory impact of SA has been reported in recent studies demonstrating the activation of defense-related genes, such as *PR-2a*, *PR-5*, *NPR*, *PO*, and *PAL*, against Fusarium wilt in tomato and watermelon [25,83], thus providing the basis for the better plant-protecting capacity of SINCs in *Fon*-infected watermelon plants. Our results demonstrated that both FeNPs and SINCs showed pronounced biological effects by inducing cellular signaling and defense mechanisms compared to their respective controls, which can be attributed to their unique physicochemical properties as well as greater bioavailability and uptake by watermelon plants. Therefore, it is suggested that the activation of defense response, primed by bio-FeNPs- and SINCs, might be responsible for the inhibition of *Fon* invasive growth within watermelon plants, rather than the direct antifungal activity of these NPs. Furthermore, SINCs have a more obvious impact on the SA-dependent plant defense system than bio-FeNPs, and can be useful for improving watermelon resistance to Fusarium wilt.

Conclusions

The present study highlights the potential of bio-FeNPs and SINCs in improving plant growth and suppressing Fusarium wilt in watermelon. The analytical techniques confirmed the synthesis of bio-FeNPs and SINCs nanocrystals with variable shapes. Greenhouse experiments demonstrated that the application of bio-FeNPs and SINCs significantly improved the growth and overall health of watermelon plants by suppressing the Fusarium wilt development *via* restricting pathogen invasion within roots and stems. Physiological and biochemical results revealed that SINCs resulted in even greater benefits than bio-FeNPs alone, with a reduction in oxidative stress markers and an improvement in enzymatic antioxidants in watermelon plants, suggesting their protective role against oxidative damage. Molecular profiling revealed that bio-FeNPs and SINCs could potentiate and induce SAR in watermelon plants by activating the expression of SA biosynthesis, signaling, and responsive genes. Based on these findings, we proposed a schematic model of the SINCs-mediated suppression of watermelon Fusarium wilt (Fig. 8). Overall, these findings provide new insights into the potential of bio-FeNPs and SINCs as biostimulants and bioprotectants in watermelon cultivation against Fusarium wilt. Further research is needed to fully understand the mechanisms of bio-Fe-based NCs in plant disease control and to determine their efficacy under field conditions.

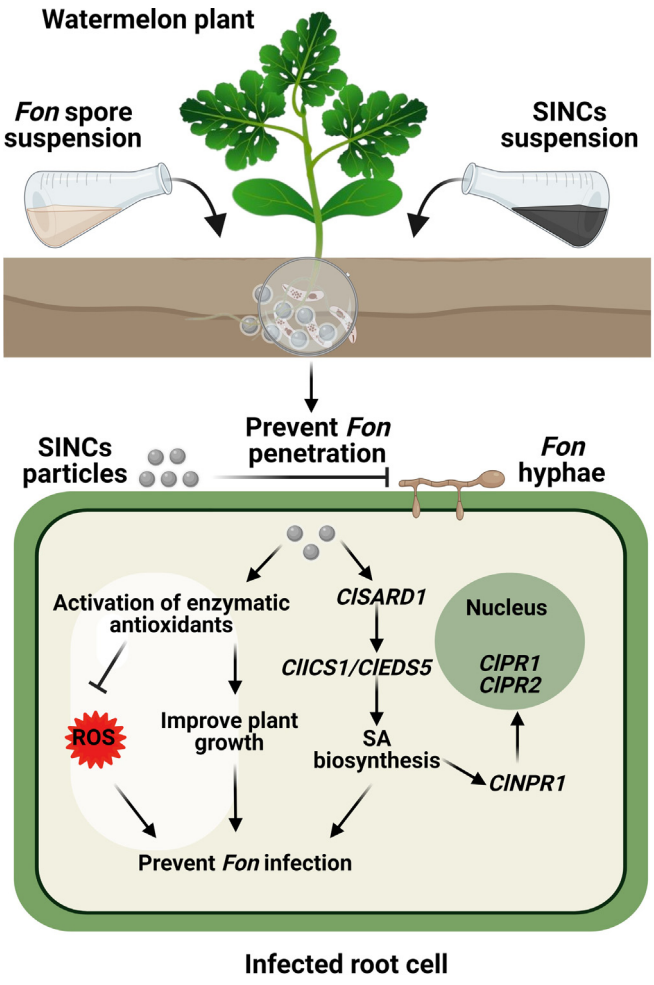

Fig. 8. Schematic illustration of watermelon Fusarium wilt suppressing mechanism of SINCs. According to the proposed model, SINCs alleviate Fusarium wilt damages in watermelon plants *via* modulating antioxidative system and inducing SAR through triggering the expression of SA signaling pathway genes, thus effectively restricting invasive growth of *Fon*.

CRediT authorship contribution statement

Muhammad Noman: Conceptualization, Methodology, Writing – original draft, Writing – review & editing. **Temoor Ahmed:** Inves-

tigation, Formal analysis, Writing – review & editing. **Muhammad Shahid:** Investigation, Formal analysis, Writing – review & editing. **Muhammad Mudassir Nazir:** Formal analysis. **Azizullah:** Investigation, Formal analysis. **Dayong Li:** Methodology, Visualization, Validation, Writing – review & editing. **Fengming Song:** Supervision, Funding acquisition, Methodology, Writing – review & editing.

Declaration of Competing Interest

The authors declare that they have no known competing financial interests or personal relationships that could have appeared to influence the work reported in this paper.

Acknowledgements

This research was supported by the Chinese Agriculture Research System of MOF and MARA of China (Grant no. CARS-25). The manuscript was written through contributions of all authors. All authors have given approval to the final version of the manuscript.

Appendix A. Supplementary data

Supplementary data to this article can be found online at https://doi.org/10.1016/j.jare.2023.06.011.

References

[1] Kang H, Elmer W, Shen Y, Zuverza-Mena N, Ma C, Botella P, et al. Silica nanoparticle dissolution rate controls the suppression of Fusarium wilt of watermelon (*Citrullus lanatus*). Environ Sci Technol 2021;55(20):13513–22.
[2] Martyn RD. Fusarium wilt of watermelon: 120 years of research. In: Janick J, editor. Horticultural Reviews. 42. New Jersey, USA: Wiley-Blackwell; 2014. p. 349–442.
[3] Elmer W, De La Torre-Roche R, Pagano L, Majumdar S, Zuverza-Mena N, Dimkpa C, et al. Effect of metalloid and metal oxide nanoparticles on Fusarium wilt of watermelon. Plant Dis 2018;102(7):1394–401.
[4] M. Noman T. Ahmed U. Ijaz A. Hameed M. Shahid Azizullah, et al. Noman M, Ahmed T, Ijaz U, Hameed A, Shahid M, Azizullah, et al. Microbe-oriented nanoparticles as phytomedicines for plant health management: An emerging paradigm to achieve global food security. Crit Rev Food Sci Nutr 2022. doi: https://doi.org/10.1080/10408398.2022.2046543.
[5] Ahmed T, Noman M, Jiang H, Shahid M, Ma C, Wu Z, et al. Bioengineered chitosan-iron nanocomposite controls bacterial leaf blight disease by modulating plant defense response and nutritional status of rice (*Oryza sativa* L.). Nano Today 2022;45:101547.
[6] Elamawi RM, Al-Harbi RE. Effect of biosynthesized silver nanoparticles on *Fusarium oxysporum* fungus the cause of seed rot disease of faba bean, tomato and barley. J Plant Prot Pathol 2014;5(2):225–37.
[7] Elmer WH, Zuverza-Mena N, Triplett LR, Roberts EL, Silady RA, White JC. Foliar application of copper oxide nanoparticles suppresses Fusarium wilt development on chrysanthemum. Environ Sci Technol 2021;55(15):10805–10.
[8] Luo X, Wang Z, Wang C, Yue L, Tao M, Elmer WH, et al. Nanomaterial size and surface modification mediate disease resistance activation in cucumber (*Cucumis sativus*). ACS Nano 2023. doi: https://doi.org/10.1021/acsnano.2c11790.
[9] Herlihy JH, Long TA, McDowell JM. Iron homeostasis and plant immune responses: Recent insights and translational implications. J Biol Chem 2020;295(39):13444–57.
[10] Win TT, Khan S, Bo B, Zada S, Fu P. Green synthesis and characterization of Fe_3O_4 nanoparticles using *Chlorella*-K01 extract for potential enhancement of plant growth stimulating and antifungal activity. Sci Rep 2021;11(1):21996.
[11] Ashraf H, Batool T, Anjum T, Illyas A, Li G, Naseem S, et al. Antifungal potential of green synthesized magnetite nanoparticles black coffee–magnetite nanoparticles against wilt infection by ameliorating enzymatic activity and gene expression in *Solanum lycopersicum* L. Front Microbiol 2022;13:31.
[12] Bilesky-José N, Maruyama C, Germano-Costa T, En C, Carvalho L, Grillo R, et al. Biogenic α-Fe_2O_3 nanoparticles enhance the biological activity of *Trichoderma* against the plant pathogen *Sclerotinia sclerotiorum*. ACS Sustain Chem Eng 2021;9(4):1669–83.
[13] Jacinto M, Silva V, Valladão D, Souto R. Biosynthesis of magnetic iron oxide nanoparticles: A review. Biotechnol Lett 2021;43:1–12.
[14] Luo J, Zhang D-x, Jing T, Liu G, Cao H, Li B-x, et al. Pyraclostrobin loaded lignin-modified nanocapsules: Delivery efficiency enhancement in soil improved control efficacy on tomato Fusarium crown and root rot. Chem Eng J 2020;394:124854.
[15] Karny A, Zinger A, Kajal A, Shainsky-Roitman J, Schroeder A. Therapeutic nanoparticles penetrate leaves and deliver nutrients to agricultural crops. Sci Rep 2018;8(1):7589.
[16] Ding P, Ding Y. Stories of salicylic acid: A plant defense hormone. Trends Plant Sci 2020;25(6):549–65.
[17] Peng Y, Yang J, Li X, Zhang Y. Salicylic acid: Biosynthesis and signaling. Annu Rev Plant Biol 2021;72:761–91.
[18] Tripathi D, Raikhy G, Kumar D. Chemical elicitors of systemic acquired resistance-Salicylic acid and its functional analogs. Curr Plant Biol 2019;17:48–59.
[19] Klessig DF, Choi HW, Dempsey DMA. Systemic acquired resistance and salicylic acid: Past, present, and future. Mol Plant Microbe Interact 2018;31(9):871–88.
[20] Bawa G, Feng L, Yan L, Du Y, Shang J, Sun X, et al. Pre-treatment of salicylic acid enhances resistance of soybean seedlings to *Fusarium solani*. Plant Mol Biol 2019;101:315–23.
[21] Narusaka Y, Narusaka M, Horio T, Ishii H. Comparison of local and systemic induction of acquired disease resistance in cucumber plants treated with benzothiadiazoles or salicylic acid. Plant Cell Physiol 1999;40(4):388–95.
[22] Yang Y-x, Wu C, Ahammed GJ, Wu C, Yang Z, Wan C, et al. Red light-induced systemic resistance against root-knot nematode is mediated by a coordinated regulation of salicylic acid, jasmonic acid and redox signaling in watermelon. Front. Plant Sci 2018;9:899.
[23] Karki K, Negi VS, Coolong T, Petkar A, Mandal M, Kousik C, et al. Micronutrients affect expression of induced resistance genes in hydroponically grown watermelon against *Fusarium oxysporum* f. sp *niveum* and *Meloidogyne incognita* Pathogens 2022;11(10):1136.
[24] Zhu F, Fang Y, Wang Z, Wang P, Yang K, Xiao L, et al. Salicylic acid remodeling of the rhizosphere microbiome induces watermelon root resistance against *Fusarium oxysporum* f. sp *niveum* infection Front Microbiol 2022;13:1015038.
[25] Zhu F, Wang Z, Su W, Tong J, Fang Y, Luo Z, et al. Study on the role of salicylic acid in watermelon-resistant Fusarium wilt under different growth conditions. Plants 2022;11(3):293.
[26] Somasegaran P, Hoben HJ. Quantifying the growth of rhizobia. In: Somasegaran P, Hoben HJ, editors. Handbook for Rhizobia. New York: Springer; 1994. p. 47–57.
[27] Wiegand I, Hilpert K, Hancock RE. Agar and broth dilution methods to determine the minimal inhibitory concentration (MIC) of antimicrobial substances. Nat Protoc 2008;3(2):163–75.
[28] Ogier J-C, Pagès S, Galan M, Barret M, Gaudriault S. *rpoB*, a promising marker for analyzing the diversity of bacterial communities by amplicon sequencing. BMC Microbiol 2019;19(1):171.
[29] Weisburg WG, Barns SM, Pelletier DA, Lane DJ. 16S ribosomal DNA amplification for phylogenetic study. J Bacteriol 1991;173(2):697–703.
[30] Noman M, Ahmed T, Hussain S, Niazi MBK, Shahid M, Song F. Biogenic copper nanoparticles synthesized by using a copper-resistant strain *Shigella flexneri* SNT22 reduced the translocation of cadmium from soil to wheat plants. J Hazard Mater 2020;398:123175.
[31] Unal B, Durmus Z, Kavas H, Baykal A, Toprak M. Synthesis, conductivity and dielectric characterization of salicylic acid–Fe_3O_4 nanocomposite. Mater Chem Phys 2010;123(1):184–90.
[32] Manjula R, Thenmozhi M, Thilagavathi S, Srinivasan R, Kathirvel A. Green synthesis and characterization of manganese oxide nanoparticles from *Gardenia resinifera* leaves. Mater Today: Proc 2020;26(4):3559–63.
[33] He F, Cai W, Lin J, Yu B, Owens G, Chen Z. Reducing the impact of antibiotics in wastewaters: Increased removal of mitoxantrone from wastewater by biosynthesized manganese nanoparticles. J Clean Prod 2021;293:126207.
[34] Kamran U, Bhatti HN, Iqbal M, Jamil S, Zahid M. Biogenic synthesis, characterization and investigation of photocatalytic and antimicrobial activity of manganese nanoparticles synthesized from *Cinnamomum verum* bark extract. J Mol Struct 2019;1179:532–9.
[35] Patra T, Mohanty A, Singh L, Muduli S, Parhi PK, Sahoo TR. Effect of calcination temperature on morphology and phase transformation of MnO_2 nanoparticles: A step towards green synthesis for reactive dye adsorption. Chemosphere 2022;288:132472.
[36] Iwunze M. Absorptiometric determination of acetylsalicylic acid in aqueous ethanolic solution. Anal Lett 2008;41(16):2944–53.
[37] Noman M, Ahmed T, Ijaz U, Shahid M, Nazir MM, White JC, et al. Bio-functionalized manganese nanoparticles suppress Fusarium wilt in watermelon (*Citrullus lanatus* L.) by infection disruption, host defense response potentiation, and soil microbial community modulation. Small 2023;19(2):2205687.
[38] Noman M, Shahid M, Ahmed T, Tahir M, Naqqash T, Muhammad S, et al. Green copper nanoparticles from a native *Klebsiella pneumoniae* strain alleviated oxidative stress impairment of wheat plants by reducing the chromium bioavailability and increasing the growth. Ecotoxicol Environ Saf 2020;192:110303.
[39] Noman M, Ahmed T, Shahid M, Niazi MBK, Qasim M, Kouadri F, et al. Biogenic copper nanoparticles produced by using the *Klebsiella pneumoniae* strain NST2 curtailed salt stress effects in maize by modulating the cellular oxidative repair mechanisms. Ecotoxicol Environ Saf 2021;217:112264.
[40] Ahmed T, Noman M, Rizwan M, Ali S, Ijaz U, Nazir MM, et al. Green molybdenum nanoparticles-mediated bio-stimulation of *Bacillus* sp. strain ZH16 improved the wheat growth by managing in planta nutrients supply, ionic homeostasis and arsenic accumulation. J Hazard Mater 2022;423:127024.

[41] Schneider K, Schlegel H. Production of superoxide radicals by soluble hydrogenase from *Alcaligenes eutrophus* H16. Biochem J 1981;193(1):99–107.
[42] Kingston-Smith A, Harbinson J, Foyer C. Acclimation of photosynthesis, H_2O_2 content and antioxidants in maize (*Zea mays*) grown at sub-optimal temperatures. Plant Cell Environ 1999;22(9):1071–83.
[43] Heath RL, Packer L. Photoperoxidation in isolated chloroplasts: I. kinetics and stoichiometry of fatty acid peroxidation. Arch Biochem Biophys 1968;125 (1):189–98.
[44] Zhang J, Kirkham M. Drought-stress-induced changes in activities of superoxide dismutase, catalase, and peroxidase in wheat species. Plant Cell Physiol 1994;35(5):785–91.
[45] Chance B, Maehly A. [136] Assay of catalases and peroxidases. Meth Enzymol 1955;2:764–75.
[46] Gao Y, Xiong X, Wang H, Wang J, Bi Y, Yan Y, et al. Ero1-Pdi1 module-catalysed dimerization of a nucleotide sugar transporter, FonNst2, regulates virulence of *Fusarium oxysporum* on watermelon. Environ Microbiol 2021;24(3):1200–20.
[47] Dai Y, Cao Z, Huang L, Liu S, Shen Z, Wang Y, et al. CCR4-Not complex subunit Not2 plays critical roles in vegetative growth, conidiation and virulence in watermelon fusarium wilt pathogen *Fusarium oxysporum* f. sp *niveum* Front Microbiol 2016;7:1449.
[48] Li B, Mao H-Y, Zhang Z-Y, Chen X-J, Ouyang S-Q. FolVps9, a guanine nucleotide exchange factor for FolVps21, is essential for fungal development and pathogenicity in *Fusarium oxysporum* f. sp *lycopersici* Front Microbiol 2019;10:2658.
[49] Livak KJ, Schmittgen TD. Analysis of relative gene expression data using real-time quantitative PCR and the $2^{-\Delta\Delta CT}$ method. Methods 2001;25(4):402–8.
[50] Steel RG, Torrie JH, Dickey DA. Principles and Procedures of Statistics: A Biological Approach. New York: McGraw-Hill; 1997.
[51] Alfryyan N, Kordy MG, Abdel-Gabbar M, Soliman HA, Shaban M. Characterization of the biosynthesized intracellular and extracellular plasmonic silver nanoparticles using *Bacillus cereus* and their catalytic reduction of methylene blue. Sci Rep 2022;12(1):12495.
[52] Jamzad M, Kamari BM. Green synthesis of iron oxide nanoparticles by the aqueous extract of *Laurus nobilis* L. leaves and evaluation of the antimicrobial activity. J Nanostructure Chem 2020;10:193–201.
[53] Fatemi M, Mollania N, Momeni-Moghaddam M, Sadeghifar F. Extracellular biosynthesis of magnetic iron oxide nanoparticles by *Bacillus cereus* strain HMH1: Characterization and *in vitro* cytotoxicity analysis on MCF-7 and 3T3 cell lines. J Biotechnol 2018;270:1–11.
[54] Hashem AH, Abdelaziz AM, Askar AA, Fouda HM, Khalil AM, Abd-Elsalam KA, et al. *Bacillus megaterium*-mediated synthesis of selenium nanoparticles and their antifungal activity against *Rhizoctonia solani* in faba bean plants. J Fungi 2021;7(3):195.
[55] Noman M, Ahmed T, White JC, Nazir MM, Li D, Song F. *Bacillus altitudinis*-stabilized multifarious copper nanoparticles prevent bacterial fruit blotch in watermelon (*Citrullus lanatus* L.): Direct pathogen inhibition, *in planta* particles accumulation, and host stomatal immunity modulation. Small 2023;19 (15):2207136.
[56] Ballottin D, Fulaz S, Souza ML, Corio P, Rodrigues AG, Souza AO, et al. Elucidating protein involvement in the stabilization of the biogenic silver nanoparticles. Nanoscale Res Lett 2016;11(1):313.
[57] Rostamizadeh E, Iranbakhsh A, Majd A, Arbabian S, Mehregan I. Green synthesis of Fe_2O_3 nanoparticles using fruit extract of *Cornus mas* L. and its growth-promoting roles in barley. J Nanostructure Chem 2020;10:125–30.
[58] Noman M, Shahid M, Ahmed T, Niazi MBK, Hussain S, Song F, et al. Use of biogenic copper nanoparticles synthesized from a native *Escherichia* sp. as photocatalysts for azo dye degradation and treatment of textile effluents. Environ Pollut 2020;257:113514.
[59] Tkach A, Matsukovich A, Krekoten N, Tabulina L, Labunov V, Radziuk D. Graphene-oxide-coated CuO nanoparticles for functionalization of acetylsalicylic acid and diclofenac. ACS Appl Nano Mater 2020;3(6):5593–604.
[60] Kasote DM, Lee JH, Jayaprakasha G, Patil BS. Seed priming with iron oxide nanoparticles modulate antioxidant potential and defense-linked hormones in watermelon seedlings. ACS Sustain Chem Eng 2019;7(5):5142–51.
[61] Cheng F, Lu J, Gao M, Shi K, Kong Q, Huang Y, et al. Redox signaling and CBF-responsive pathway are involved in salicylic acid-improved photosynthesis and growth under chilling stress in watermelon. Front Plant Sci 2016;7:1519.
[62] Koo YM, Heo AY, Choi HW. Salicylic acid as a safe plant protector and growth regulator. Plant Pathol J 2020;36(1):1–10.
[63] Rivas-San Vicente M, Plasencia J. Salicylic acid beyond defence: Its role in plant growth and development. J Exp Bot 2011;62(10):3321–38.
[64] Raju D, Mehta UJ, Beedu SR. Biogenic green synthesis of monodispersed gum kondagogu (*Cochlospermum gossypium*) iron nanocomposite material and its application in germination and growth of mung bean (*Vigna radiata*) as a plant model. IET Nanobiotechnol 2016;10(3):141–6.
[65] Asgari-Targhi G, Iranbakhsh A, Ardebili ZO, Tooski AH. Synthesis and characterization of chitosan encapsulated zinc oxide (ZnO) nanocomposite and its biological assessment in pepper (*Capsicum annuum*) as an elicitor for *in vitro* tissue culture applications. Int J Biol Macromol 2021;189:170–82.
[66] Ghassemi-Golezani K, Abdoli S. Improving ATPase and PPase activities, nutrient uptake and growth of salt stressed ajowan plants by salicylic acid and iron-oxide nanoparticles. Plant Cell Rep 2021;40:559–73.
[67] Souri Z, Karimi N, Sarmadi M, Rostami E. Salicylic acid nanoparticles (SANPs) improve growth and phytoremediation efficiency of *Isatis cappadocica* Desv., under As stress. IET Nanobiotechnol 2017;11(6):650–5.
[68] Cao X, Wang C, Luo X, Yue L, White JC, Elmer W, et al. Elemental sulfur nanoparticles enhance disease resistance in tomatoes. ACS Nano 2021;15 (7):11817–27.
[69] Shang H, Ma C, Li C, White JC, Polubesova T, Chefetz B, et al. Copper sulfide nanoparticles suppress *Gibberella fujikuroi* infection in rice (*Oryza sativa* L.) by multiple mechanisms: Contact-mortality, nutritional modulation and phytohormone regulation. Environ Sci. Nano 2020;7(9):2632–43.
[70] Ma C, Borgatta J, Hudson BG, Tamijani AA, De La Torre-Roche R, Zuverza-Mena N, et al. Advanced material modulation of nutritional and phytohormone status alleviates damage from soybean sudden death syndrome. Nat Nanotechnol 2020;15(12):1033–42.
[71] Giannousi K, Avramidis I, Dendrinou-Samara C. Synthesis, characterization and evaluation of copper based nanoparticles as agrochemicals against *Phytophthora infestans*. RSC Adv 2013;3(44):21743–52.
[72] Shah IH, Ashraf M, Khan AR, Manzoor MA, Hayat K, Arif S, et al. Controllable synthesis and stabilization of *Tamarix aphylla*-mediated copper oxide nanoparticles for the management of Fusarium wilt on musk melon. 3 Biotech 2022;12(6):128.
[73] Bektas Y, Eulgem T. Synthetic plant defense elicitors. Front Plant Sci 2015;5:804.
[74] Abdelaziz AM, Elshaer MA, Abd-Elraheem MA, Ali OMOM, Haggag MI, El-Sayyad GS, et al. *Ziziphus spina-christi* extract-stabilized novel silver nanoparticle synthesis for combating *Fusarium oxysporum*-causing pepper wilt disease: *In vitro* and *in vivo* studies. Arch Microbiol 2023;205(2):69.
[75] Michielse CB, Rep M. Pathogen profile update: *Fusarium oxysporum*. Mol Plant Pathol 2009;10(3):311–24.
[76] T. Ahmed H. Ren M. Noman M. Shahid M. Liu M.A. Ali et al. Ahmed T, Ren H, Noman M, Shahid M, Liu M, Ali MA, et al. Green synthesis and characterization of zirconium oxide nanoparticles by using a native *Enterobacter* sp. and its antifungal activity against bayberry twig blight disease pathogen *Pestalotiopsis versicolor*. NanoImpact 2021;21:100281.
[77] Biswas A, Vanlalveni C, Lalfakzuala R, Nath S, Rokhum L. *Mikania mikrantha* leaf extract mediated biogenic synthesis of magnetic iron oxide nanoparticles: Characterization and its antimicrobial activity study. Mater Today: Proc 2021;42:1366–73.
[78] El-Hady NAAA, El-Sayed AI, El-Saadany SS, Deligios PA, Ledda L. Exogenous application of foliar salicylic acid and propolis enhances antioxidant defenses and growth parameters in tomato plants. Plants 2021;10(1):74.
[79] Ashraf H, Anjum T, Riaz S, Batool T, Naseem S, Li G. Sustainable synthesis of microwave-assisted IONPs using *Spinacia oleracea* L. for control of fungal wilt by modulating the defense system in tomato plants. J Nanobiotechnol 2022;20 (1):8..
[80] Mandal S, Mallick N, Mitra A. Salicylic acid-induced resistance to *Fusarium oxysporum* f. sp. *lycopersici* in tomato. Plant Physiol Biochem 2009;47 (7):642–9.
[81] Saleem M, Fariduddin Q, Castroverde CDM. Salicylic acid: A key regulator of redox signalling and plant immunity. Plant Physiol Biochem 2021;168:381–97.
[82] Wani AB, Chadar H, Wani AH, Singh S, Upadhyay N. Salicylic acid to decrease plant stress. Environ Chem Lett 2017;15:101–23.
[83] Chakraborty N. Salicylic acid and nitric oxide cross-talks to improve innate immunity and plant vigor in tomato against *Fusarium oxysporum* stress. Plant Cell Rep 2021;40(8):1415–27.